

Chapter

Mathematical Models of Serotonin, Histamine, and Depression

Janet Best, Anna Marie Buchanan, Herman Frederik Nijhout, Parastoo Hashemi and Michael C. Reed

Abstract

The coauthors have been working together for ten years on serotonin, dopamine, and histamine and their connection to neuropsychiatric illnesses. Hashemi has pioneered many new experimental techniques for measuring serotonin and histamine in real time in the extracellular space in the brain. Best, Reed, and Nijhout have been making mathematical models of brain metabolism to help them interpret Hashemi's data. Hashemi demonstrated that brain histamine inhibits serotonin release, giving a direct mechanism by which inflammation can cause a decrease in brain serotonin and therefore depression. Many new biological phenomena have come out of their joint research including 1) there are two different reuptake mechanisms for serotonin; 2) the effect of the serotonin autoreceptors is not instantaneous and is long-lasting even when the extracellular concentrations have returned to normal; 3) that mathematical models of serotonin metabolism and histamine metabolism can explain Hashemi's experimental data; 4) that variation in serotonin autoreceptors may be one of the causes of serotonin-linked mood disorders. Here we review our work in recent years for biological audiences, medical audiences, and researchers who work on mathematical modeling of biological problems. We discuss the experimental techniques, the creation and investigation of mathematical models, and the consequences for neuropsychiatric diseases.

Keywords: serotonin, histamine, depression, mathematical model

1. Introduction

It is worthwhile to begin by reminding ourselves that the question of depression and the brain is so difficult because the brain consists of many different systems that interact with each other. First is the **electrophysiology** of the brain including the biophysics of individual neurons and the behavior of neural networks. Second is the **biochemistry** of the brain, not just cell biochemistry and the structure and function of receptors, but also the fact that many brain neurons do not do one-to-one signaling with other neurons. These neurons, like the serotonin (5-HT) neurons of the dorsal raphe nucleus (DRN) have dense projections to other brain regions in which their axons have myriad varicosities that release the transmitter when the neuron fires, thus changing the concentration of the transmitter in the extracellular space of the projection region. In a sense, these neurons project changes in

biochemistry over long distances in the brain. Example are the 5-HT projections from the DRN to the striatum and the dopamine projection from the substantia nigra to the striatum. Third is the **genomics** of the brain, not just the genotypes of individuals but also how gene expression levels vary depending on electrophysiology, biochemistry, and the other systems below. Fourth is the **endocrine** system. The brain is an endocrine organ itself but is also influenced by other endocrine organs such as the ovaries and the adrenal glands. Fifth, the brain is affected by the current status of the **immune system** that affects the release of histamine from mast cells. Sixth, the brain creates **behavior** but behavior affects the endocrine and biochemical systems. And, these six systems operate on a wide range of spatial and temporal scales.

There are four additional difficulties. The brain is not fixed like a machine, but is dynamically changing on short and long time scales based on its challenges and history of challenges. Secondly, direct *in vivo* experimentation on humans is unethical, so one is left with remote sensing (imaging, drug responses, etc.) and extrapolation from animal experiments often performed on tissue slices. Third, there is an exceptional amount of individual variation. For example, it is known that gene expression levels vary by about 25% from person to person [1–3] and of course vary in time; so what does it mean to speak of “the brain?” Finally, not surprisingly, a myriad of homeostatic mechanisms (such as 5-HT_{1B} autoreceptors on 5-HT varicosities) have evolved so that the brain can keep functioning “normally”, despite changing inputs, gene polymorphisms, and enormous biological variation. These mechanisms, whether gene regulatory networks or biochemical regulatory motifs, operate over limited scales and are almost always nonlinear, and this makes guessing the likely results of interventions very difficult.

In this situation where the system is complex and experimentation is difficult, mathematical modeling can provide a useful tool. A model gives voice to our assumptions about how something works. Every biological experiment is designed within the context of a conceptual model and its results cause us to confirm, reject, or alter that model. Conceptual models are always incomplete because biological systems are very complex and incompletely understood. Moreover, and as a purely practical matter, experiments tend to be guided by small conceptual models of only a very small part of a system, with the assumption (or hope) that the remaining details and context do not matter or can be adequately controlled. Mathematical models are formal statements of conceptual models. Like conceptual models, they are typically incomplete and tend to simplify some details of the system. But what they do have, which experimental systems do not, is that they are completely explicit about what is in the model, and what is not. Having a completely defined system has the virtue of allowing one to test whether the assumptions and structure of the model are sufficient to explain the observed results. The purpose of mathematical models is not just to match extant experimental or clinical data, but to provide an *in silico* platform for experimentation and investigation of system behavior. Such experiments are quick and inexpensive and so are particularly useful for testing hypotheses. Of course, to be useful, mathematical models should be based as much as possible on the underlying physiology.

Janet Best is a mathematician at Ohio State, Michael Reed is a mathematician at Duke University and H. Frederik Nijhout is a biologist at Duke. They have been working together on brain metabolism since 2008. They began by creating a large mathematical model of dopamine (DA) synthesis, storage in vesicles, catabolism, release, reuptake and control in synapses and varicosities [4] and a similar model for serotonin [5]. They used these models (and simpler ones) to study many phenomena, including passive and active stabilization of DA in the striatum [6], the role of 5-HT in the striatum [7], and the interaction of DA and 5-HT in the striatum

in levodopa therapy for Parkinson's disease [8, 9]. Their papers on brain metabolism are available on the website sites.duke.edu/metabolism.

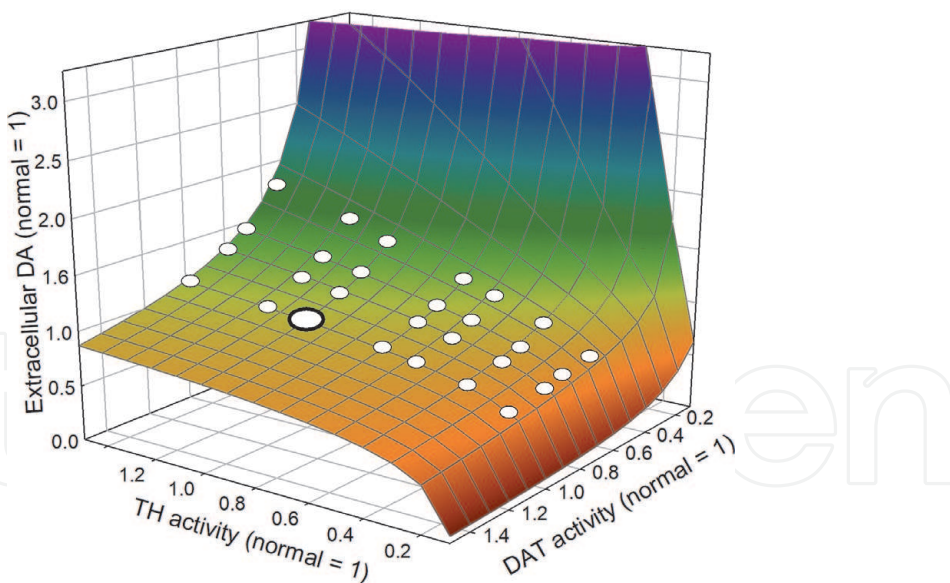
Parastoo Hashemi is an electrochemist and biomedical engineer at Imperial College London and the University of South Carolina. She was the first experimentalist to be able to measure the time course of 5-HT concentration and histamine concentration in the extracellular space of the brain *in vivo* [10]. In 2013, she contacted Best, Reed, and Nijhout and asked for help interpreting the results of her experiments, and the four us have been actively collaborating since then. All of our joint papers are available on the above website. Our collaboration always begins by active discussion of new experimental results that often change our previous understanding and therefore require changing previous models. The new models then often suggest new experiments to test new hypotheses that come from model experimentation. In this review, there will be many examples of this back and forth between experiment and modeling that we have found to be very productive. Anna Marie Buchanan is a graduate student in the Department of Chemistry and Biochemistry at the University of South Carolina.

In Section 2 we discuss the importance of homeostatic mechanisms in the brain. In Section 3 we discuss our first modeling paper with the Hashemi Lab [11]. That paper changed our understanding of 5-HT_{1b} autoreceptors and showed that the way we modeled autoreceptors in 2010 [5] was wrong. Section 4 describes our 2017 paper [12] creating a mathematical model for histamine dynamics in the brain and Section 5 discusses our 2020 paper [13] revising and expanding our original 5-HT model. In Section 6 we briefly describe the techniques for measuring 5-HT and histamine in the extracellular space and in Section 7 we describe our ideas and speculations about depression. Lastly, in Section 8 we discuss future work.

2. Homeostatic mechanisms

The extracellular space occupies a significant portion of brain volume and is extremely important. Not only is it the medium by which nutrients in the plasma are delivered to brain cells but it is also an important medium for communication between cells. Thus, it is not surprising that a variety of mechanisms have evolved to control the extracellular concentrations of neurotransmitters in different brain regions within fairly narrow limits. For example, DA is synthesized from tyrosine by tyrosine hydroxylase (TH) and TH shows substrate inhibition as does tryptophan hydroxylase (TPH) that synthesizes 5-HT from tryptophan. And, the concentration of DA in the extracellular space inhibits both synthesis and release of DA via the DA autoreceptors, a kind of end product inhibition. Similar mechanisms exist for 5-HT via the 5-HT autoreceptors. We will discuss the 5-HT autoreceptors in detail later. Our purpose here is to show what this homeostasis looks like and what the consequences are for DA.

The main determinants of the DA concentration in the extracellular space are rate of release from synapses and varicosities and rate of reuptake by the dopamine transporters (DATs). Release is dependent on the rate of synthesis via TH. **Figure 1** shows the concentration of DA in the extracellular space as a function of TH activity and DAT activity, computed by our 2009 mathematical model [4]. The normal steady state of the model is indicated by the large white dot that corresponds to 100% TH and DAT activity. The genes for TH and DAT have many common polymorphisms in the human population. The steady state extracellular DA concentration for combinations of these polymorphisms are shown by the small white circles on the surface. It's quite amazing, but all these points are on the homeostatic (approximately flat) part of the surface. Even though these polymorphisms are

**Figure 1.**

Dependence of extracellular DA on TH and DAT activity. The large white dot shows the extracellular DA concentration when TH and DAT have normal activity, where, for each variable, normal is scaled to 1. The normal steady state is in the middle of a large relatively flat plateau, extracellular DA does not change much as TH and DAT activity vary. The small white dots show the steady states for different combinations of TH and DAT polymorphisms common in the human population. Though these polymorphisms are functional, in that they have large effects on activity, they do not affect extracellular DA very much. This homeostatic effect is created by the dopamine autoreceptors.

functional, that is they have big effects on the activities of TH and DAT, they do not affect the extracellular concentration of DA very much. This homeostasis is created by the above two mechanisms, substrate inhibition and the autoreceptors. From an evolutionary point of view maybe the fact that the steady states for the polymorphisms are on the flat part of the surface is not surprising. If a polymorphism pushed the steady up the blue cliff in the back (as in cocaine addiction) or off the orange cliff in the right front (as in Parkinson's disease) then that polymorphism would not likely be common in the human population. It's interesting to consider the row of polymorphism steady states nearest the orange cliff. They are on the homeostatic part of the surface, but barely. One could think of them as "predisposed" to low DA diseases. In fact, individuals with this low TH activity polymorphism often show muscle dystonia and other symptoms of low DA [14]. The surface in **Figure 1** was computed assuming variation in TH and DAT, but there are many other variables in the system, for example monoamine oxidase (MAO), and variations in those variables could change the locations of the white dots.

The point is that the existence of homeostatic mechanisms make linear arguments that assume that a large change in one variable automatically results in large changes in downstream variables both simplistic and often wrong. Therefore, it is important to investigate and understand homeostatic mechanisms in the brain and their consequences.

3. Revised understanding of serotonin dynamics

Efforts to understand the serotonergic system and in particular the clearance dynamics of serotonin date back decades, but results were limited by experimental technology. Only recently has the Hashemi Lab been able to measure serotonin concentrations in the extracellular space *in vivo*. With early fast scan cyclic voltammetry (FSCV, see Section 6) experiments, the Wightman lab was able to measure release and clearance of serotonin in electrically stimulated rat brain slices

[15]. The data were fit to a simple model for release and Michaelis–Menten reuptake of serotonin. Further experimental innovation enabled Hashemi to evoke the release of serotonin upon stimulation of the medial forebrain bundle (MFB), and measure the release and clearance *in vivo* in rat substantia nigra pars reticulata (SNr). In an early paper, average release and clearance data for five mice was fit with the Wightman model for release and reuptake [10].

Subsequent efforts in mice to elucidate the serotonergic system with its response to antidepressants and autoreceptor antagonists revealed that serotonin responses are actually heterogeneous, and that averaging the responses obscures potentially important phenomena [11]. Furthermore, some of the data could not be fit well with the Wightman model, as the K_m value appeared to change during the thirty second experiment. These data were the impetus for Hashemi to contact modelers Best, Reed, and Nijhout to suggest collaboration.

The mouse SNr data showed three distinct serotonin responses to a standard MFB stimulation, primarily differentiated by the clearance slopes, motivating our adoption of the terminology fast, slow, and hybrid. All three responses have a rapid rise. Fast responses are characterized by a rapid return to baseline, while slow responses show a more gradual, linear, return to baseline. Hybrid responses have both fast and slow attributes, descending rapidly for a short time and then switching to a slower decay. See **Figure 2**.

Our model, shown below, employs release and Michaelis–Menten clearance kinetics similar to the Wightman model. However, our model additionally incorporates a second reuptake mechanism, a basal concentration of serotonin, and autoreceptor effects. $[S(t)]$ denotes the concentration of serotonin in the SNr extracellular space. We assume that $[S(t)]$ satisfies the differential equation:

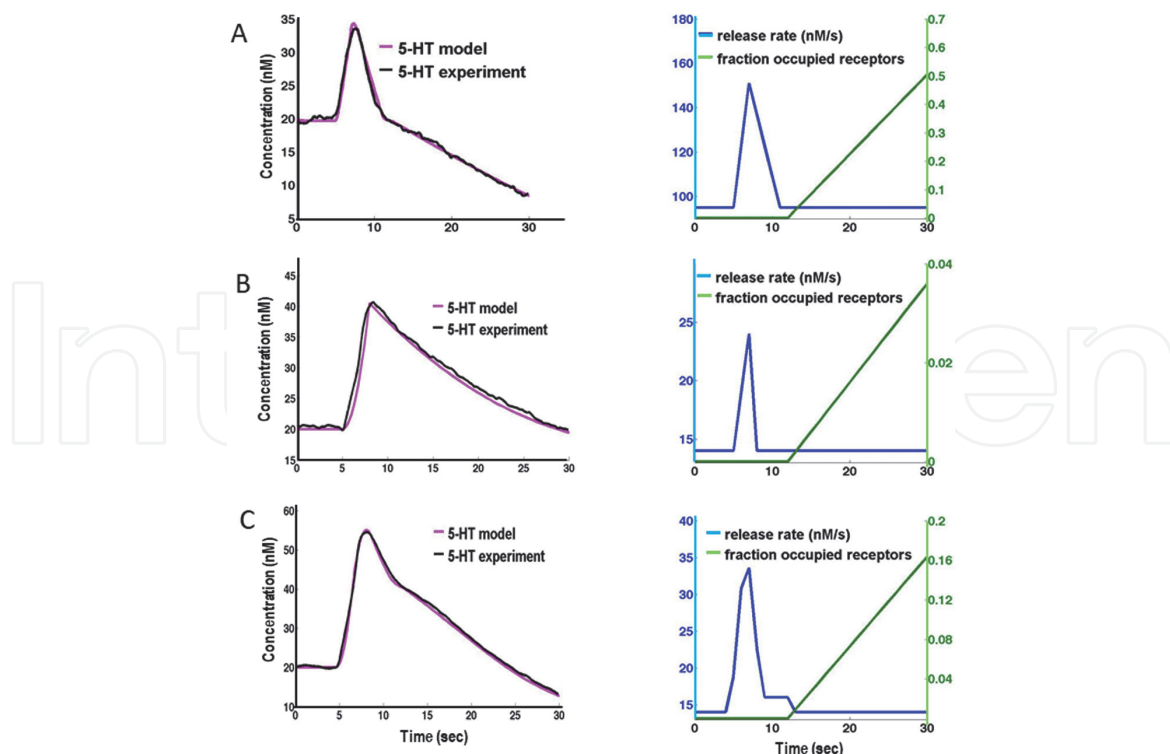


Figure 2.
*Fast, slow, and hybrid responses. The three panels on the left show fast (A), slow (B), and hybrid (C) responses measured in the SNr after stimulation of the MFB [11]. The blue curves are experimental data and the red curves come from a simple mathematical model in which the auto receptor effect was changed as a function of time (green curves in the right panels). The data and the modeling provided the first *in vivo* evidence of two distinct reuptake mechanisms for 5-HT and also showed that autoreceptor effects are long lasting and continue after 5-HT concentrations have returned to baseline.*

$$\frac{dS(t)}{dt} = R(t)(1 - A(t)) - \alpha \frac{V_{max1}[S(t)]}{K_{m1} + [S(t)]} - \beta \frac{V_{max2}[S(t)]}{K_{m2} + [S(t)]} \quad (1)$$

where $R(t)$ is the rate of release and $A(t)$ is the fraction of stimulated autoreceptors. $R(t)$ represents the neuronal firing in the DRN upon stimulation of the MFB and subsequent release of serotonin in the SNr. Firing rises and decays quickly (but not instantaneously) in response to the stimulation due to the non-instantaneous excitation/relaxation of the MFB-DRN-SNr circuitry. The two Michaelis-Menten reuptake mechanisms have different V_{max} and K_m values. V_{max1} and K_{m1} correspond to slow responses, while V_{max2} and K_{m2} correspond to fast responses. The constants α and β are the weights of the two reuptake mechanisms. For fast responses $\alpha = 0$ and $\beta = 1$, for slow responses $\alpha = 1$ and $\beta = 0$. For hybrid responses, α is taken as 1 at all times, while we incorporate β in a graded, concentration-dependent manner. When $[S(t)]$ is > 44 nM, β is 0.03 and then decays linearly to 0 as $[S(t)]$ decreases from 44 nM to 39 nM and $\beta = 0$ when $[S(t)]$ is < 39 nM, meaning that the reuptake associated with β is low affinity and so loses effectiveness at low concentrations. Thus hybrid responses have contributions from both reuptake mechanisms.

Figure 2 shows the model curves (magenta) superimposed onto the three experimental serotonin response types (black). We found that the following V_{max} and K_m values fit well to the experimental data: $V_{max1} = 17.5$ nM s $^{-1}$, $K_{m1} = 5$ nM and $V_{max2} = 780$ nM s $^{-1}$, and $K_{m2} = 170$ nM, respectively. These values were fixed for all simulations while the choices of α , β differed as indicated above. These K_m and V_{max} values agree remarkably well with high affinity, low efficiency (Uptake 1) and low affinity, high efficiency (Uptake 2) as had been suggested by Snyder and colleagues [16]. Daws and colleagues verified pharmacologically that Uptake 1 is likely to occur primarily via serotonin transporters (SERTs) on serotonergic neurons and Uptake 2 includes other transporters on other cells including the dopamine transporter, the norepinephrine transporter, and the organic cation transporter [17, 18]. Our dataset, reviewed here, was the first endogenous, *in vivo* data to support the concept of these two distinct uptake mechanisms for serotonin. We remark that the Uptake 2 parameters that worked well for us are exactly the parameters used by Shaskan and Wightman to match their experimental data. Note that the Uptake 1 parts of the response curves are quite linear, which shows that the SERTs are saturated.

The $R(t)$ and $A(t)$ functions for each response are shown in **Figure 2**. We assume that in each case the baseline concentration of 5-HT in the extracellular space is 20 nM. For all three response types, we found that the model fit well with the autoreceptor effect increasing linearly after 12 sec and continuing through the end of the 30 sec experiment. To test our model's suggestion of autoreceptor control experimentally, we treated mice with methiothepin, a non-selective serotonin receptor antagonist with highest affinity for the serotonin autoreceptors [19]. We were able to fit the data with the hybrid model, setting the autoreceptor function $A(t)$ to zero. In our previous model [5], the autoreceptor effect was an instantaneous response to the current extracellular serotonin concentration. Modeling this data revealed that the autoreceptor response differs from our earlier model in two important ways: it is not instantaneous, and it lasts well beyond when the extracellular serotonin concentration returns to baseline; see **Figure 2**. These observations motivated us to improve our autoreceptor model, see Sections 4 and 5, although we would also learn that the autoreceptors were not solely responsible for these effects in the data. Note that in Panels A and C the concentration is well below baseline at $t = 30$ and still decreasing. We will come back to this issue in Section 5.

4. A model for histamine with new autoreceptors

Histamine is a small molecule that plays an important role in the immune system [20]. In the brain, histamine is stored in mast cells and other non-neuronal cells (containing roughly half of brain histamine [21, 22]), but it also occurs as a neurotransmitter [23]. The neuronal cell bodies are in the tuberomammillary nucleus of the hypothalamus and these neurons send projections throughout the CNS, in particular to the cerebral cortex, amygdala, basal ganglia, hippocampus, thalamus, retina, and spinal cord [20]. Histamine neurons make few synapses, but release histamine from the cell bodies and from varicosities when the neurons fire. Thus the histamine neural system modulates and controls the histamine concentration in projection regions [23].

Understanding the control of histamine in the extracellular space is important because we have shown that the release of histamine inhibits 5-HT release in the hypothalamus [24]. We stimulated the MFB and measured histamine and 5-HT simultaneously in the extracellular space of the hypothalamus *in vivo* in mice; see **Figure 3**. In Panel (a), the blue curve shows the average histamine curve in the extracellular space for 5 animals. The curve peaks shortly after the 2 second

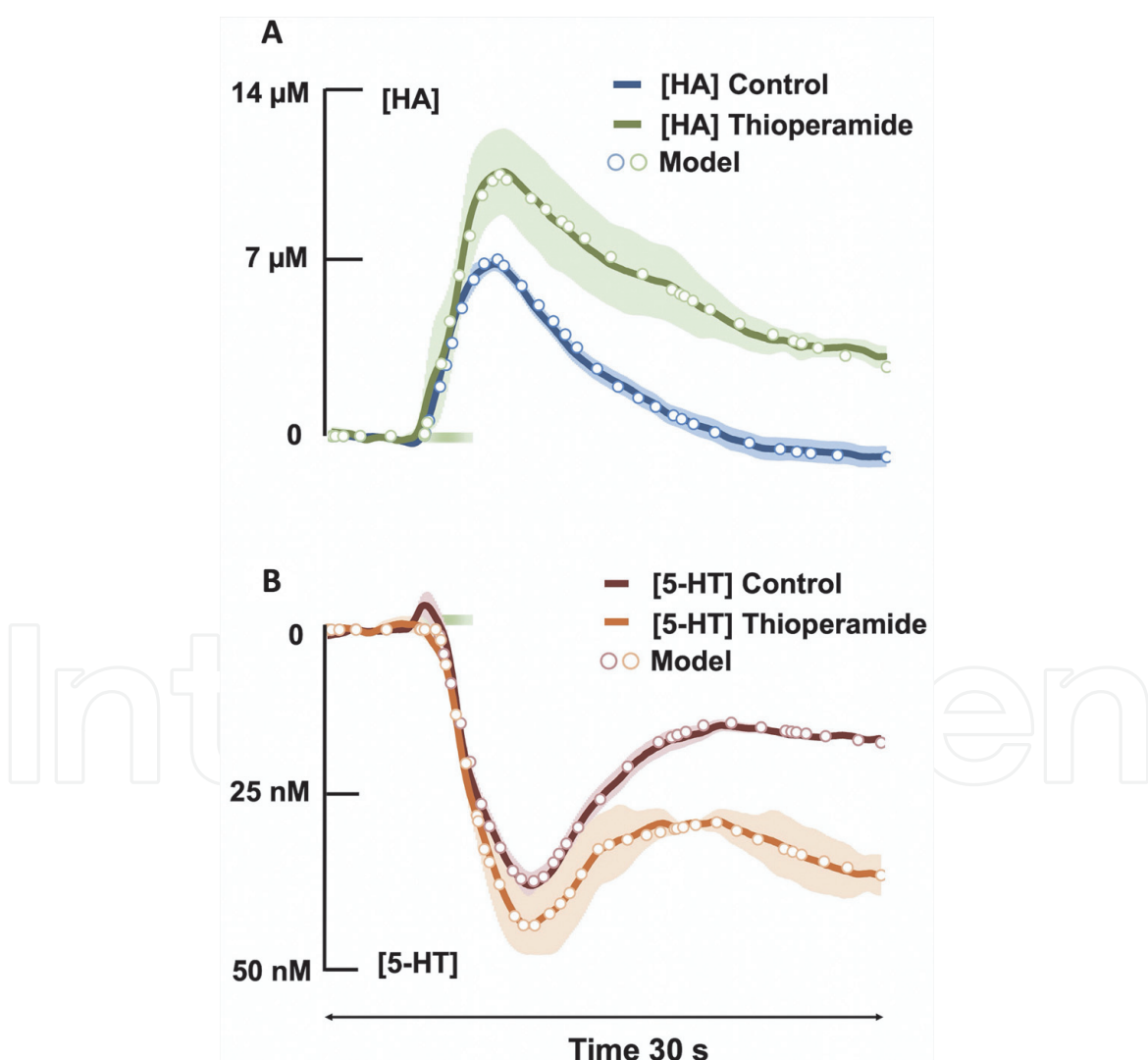


Figure 3.
Histamine inhibits 5-HT. Stimulation of the MFB releases histamine but not 5-HT in the hypothalamus. The blue curve in (A) shows extracellular histamine as a function of time and the maroon curve in (B) shows the corresponding inhibition of 5-HT release. 5-HT does not return to baseline even after histamine has returned to baseline because of the long-lasting effect of the H_3 histamine receptors on 5-HT varicosities. The green and orange curves show the histamine and 5-HT responses in the presence of thioperamide, a potent H_3 antagonist. Error bars showing SEM ($n = 5 \pm \text{SEM}$) are lighter versions of the respective colors. Horizontal bars at 0 μM and 0 nM indicate the timing of the stimulus. Predictions of a simple mathematical model are shown by the dots.

stimulation from $t = 5$ sec to $t = 7$ sec, and then descends to slightly below baseline by $t = 30$ sec. Clearance of histamine from the extracellular space is likely due to its recycling via transport back into the cytosol. While such a histamine transporter has not been identified, our unpublished experimental data shows that it is hard to deplete vesicular stores, strongly suggesting that extracellular histamine must be reuptaken into the cytosol. As we will see, the descent below baseline is caused by H_3 receptors on the histamine varicosities that inhibit histamine release. Simultaneous average measurement of 5-HT in the extracellular space is shown by the maroon curve in Panel (b). As the histamine curve peaks in Panel (a), the 5-HT curve plunges in Panel (b). As the histamine recovers to baseline in Panel (a), the 5-HT curve in Panel (b) rebounds partway towards baseline and then levels off below baseline. It is known that there are histamine H_3 receptors on 5-HT neurons that inhibit 5-HT release [25, 26]. These curves show that the effect is long-lasting. In order to test these ideas, we redid the experiments in the presence of thioperamide, a potent H_3 receptor antagonist [27]. Now the histamine curve (green) in Panel (a) goes up higher and descends more slowly. The corresponding orange 5-HT curve in Panel (b) descends even further and rebounds less. Its complicated behavior probably results from two competing influences: histamine concentration is higher but thioperamide also partially blocks the H_3 receptors on the 5-HT varicosity. The white dots come from a simple mathematical model in which we adjusted the strengths of H_3 receptor effects on both of the varicosities by hand. The fact that we could match these curves by doing that provided further confirmation that the results of the experiments were due to H_3 receptors. We note that the scales in Panels (a) and (b) are very different, μM and nM .

These experiments and their interpretation provide a likely mechanism by which the neuroinflammation that occurs in a variety of disorders could cause depression. We therefore concluded that it was important to construct a full model of the synthesis, vesicular storage, release and reuptake of histamine, and control in the extracellular space by histamine autoreceptors [12]. Overall, this model is similar to the model that we constructed for serotonin [5]. In the case of both neurotransmitters, autoreceptors on the surfaces of varicosities inhibit release when the extracellular concentration is high and diminish the inhibition when the extracellular concentration is low; this is clearly a mechanism to stabilize the extracellular concentration. In our original serotonin paper [5], we modeled this inhibition to be instantaneous as a phenomenological response to the current concentration of neurotransmitter in the extracellular space. However, as described in the previous section, our FSCV data and modeling [11] showed that autoreceptor effects are long-lasting and persist even when the concentration in the extracellular space has returned to normal. This is almost certainly because the cellular machinery that creates the inhibition and the decay of that machinery take time. Therefore, in our histamine model we introduced a minimal mathematical model of signal transduction at the G-protein coupled autoreceptor consisting of a G-protein subunit and a regulator of G-protein signaling (RGS) protein.

Figure 4 shows a schematic of the model. The pink boxes indicate substrates that are variables in the model and the gray ovals contain the acronyms of enzymes and transporters. Histidine in the blood (bHT) is transported into the varicosity by the histidine transporter (HTL) where it becomes cytosolic histidine (cHT) or goes into the histidine pool ($HTpool$). Most of the histidine that enters the cell is used for other processes than making histamine and that is what the $HTpool$ represents. cHT is converted to cytosolic histamine, cHA , by the enzyme histidine decarboxylase, $HTDC$. Some cHA is catabolized by the enzyme histamine methyltransferase, $HNMT$, some is transported into the vesicles by the monoamine transporter, MAT , and becomes vesicular histamine, vHA , and some leaks out of the cytosol into the

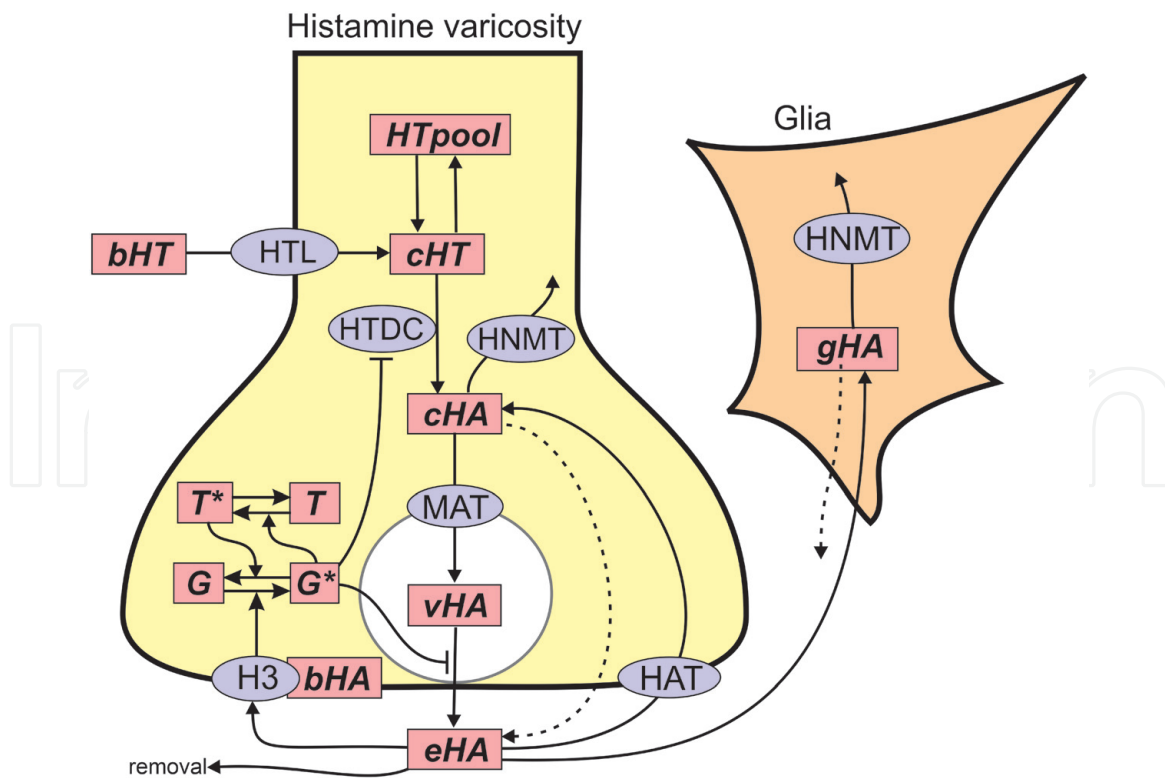


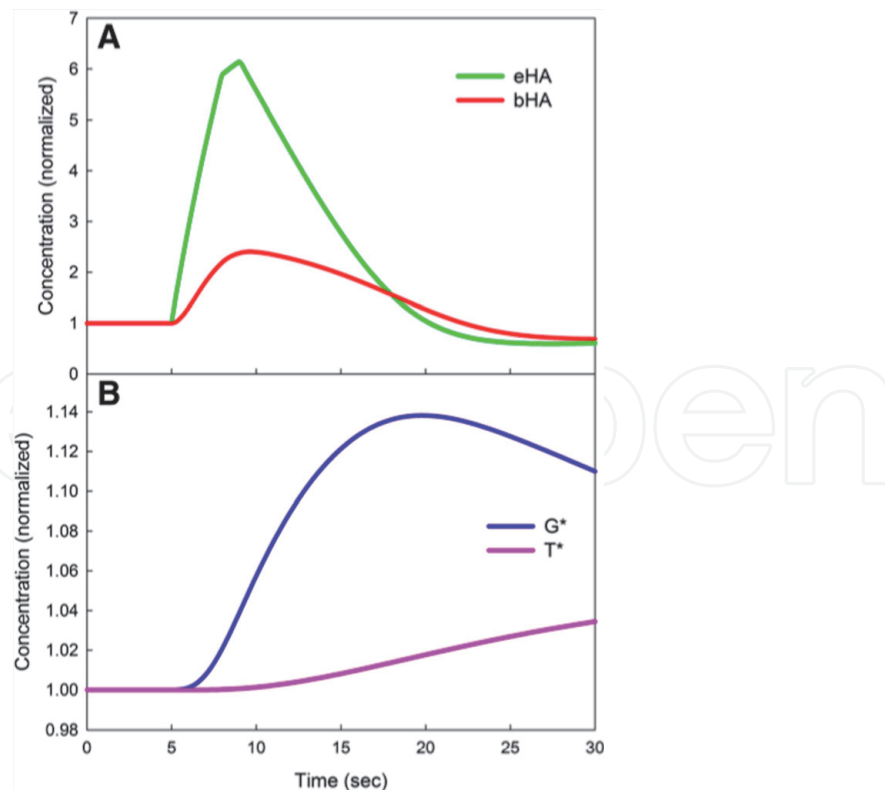
Figure 4.

Schematic of the mathematical model for histamine. bHT and cHT represent blood histidine and cytosolic histidine, respectively. cHA , vHA , eHT , $H_3 - bHA$, and gHA represent cytosolic histamine, vesicular histamine, extracellular histamine, histamine bound to autoreceptors, and glial histamine, respectively. G^* and G represent activated and inactivated autoreceptor G -proteins and T^* and T represent activated and inactivated regulators of G -proteins. Names of enzymes and transporters are as follows: HTL , the histidine transporter; $HTDC$, histidine decarboxylase; $HNMT$, histamine methyltransferase; HAT , the putative histamine transporter; H_3 , histamine autoreceptor; $HTpool$, the histidine pool.

extracellular space (indicated by the dashed line). vHA is released into the extracellular space, at a rate proportional to neuronal firing, where it becomes extracellular histamine, eHA . In the extracellular space, eHA has several fates. It can be transported back into the cytosol by a putative histamine transporter, HAT . It can diffuse away (removal). It can be transported into glial cells where it becomes glial histamine, gHA , which then leaks out or is catabolized by $HNMT$. Finally, eHA can bind to the H_3 histamine autoreceptor. The concentration of histamine bound to the autoreceptor, bHA , stimulates the conversion of the G -protein subunit, G , to its activated state, G^* . And, G^* stimulates the conversion of the RGS protein, T , to its activated state, T^* , in which it facilitates the conversion of G^* back to G . It is the activated G -protein subunit, G^* , that inhibits release and synthesis of histamine. We remark that we only track T^* and G^* since total G -protein, $G + G^*$, is assumed constant, as is $T + T^*$.

The H_3 histamine receptor (the autoreceptor in this case) is in the rhodopsin family of G -protein coupled receptors [28]. The binding of an extracellular histamine molecule to the autoreceptor causes the release of a G -protein subunit that stimulates a signaling cascade that results in inhibition of release and synthesis. Most G -protein signals are limited by RGS molecules that stimulate the G -protein subunit to rebind [29]. In our minimal model, G represents $G_\alpha - GDP$ (the inactive G -protein subunit) and G^* represents $G_\alpha - GTP$ (the signaling G -protein unit). Similarly, T represents the inactive RGS protein and T^* represents the active RGS protein.

In our model, b_0 is the total concentration of autoreceptors and bHA is the concentration of receptors bound to eHA . Normally, G and G^* are in equilibrium and their sum is constant (g_0). The concentration of bound autoreceptors (bHA)

**Figure 5.**

Autoreceptor variable dynamics in the model after stimulation. Release of histamine causes extracellular histamine to rise and then descend as histamine is transported back into the cytosol and into glial cells (green curve in A). The rise in eHA causes the concentration of bound autoreceptors to rise (red curve in Panel A). The rise in bHA causes activation of G-proteins that inhibit release and synthesis of histamine (blue curve in Panel B). The rise in G^ activates the G-protein regulator, T^* (pink curve in Panel B) and T^* starts to deactivate G^* . It is this dynamics that causes the H_3 receptor effect to be long-lasting.*

drives the equilibrium towards G^* . Similarly, T and T^* are at equilibrium and their sum is a constant (t_0). G^* drives the equilibrium towards T^* . T^* , in turn, drives the equilibrium between G and G^* back towards G . The concentration of G^* affects the release of histamine from the vesicular compartment through the function $inhib(G^*) = 2.4015 - (2.45)G^*$, and this same function appears in the formula for the velocity of the synthesis reaction (HTDC). Since $G^* = .6945$ at equilibrium, tonically the inhibition is 0.7. As $G^*(t)$ rises the inhibition gets stronger and if $G^*(t)$ decreases the inhibition becomes weaker.

The shape of the model prediction for eHA reflects the dynamics of bHA, G^* , and T^* . These curves are depicted in Figure 5 along with the graph of eHA. As one can see, eHA goes up first, followed by an increase in bHA, the concentration of bound autoreceptors. This causes a rise in G^* that in turn causes a rise in T^* that makes G^* start to decline. The inhibition of release given by the function $inhib(G^*)$ depends on G^* as described above. This is the long-lasting autoreceptor effect. The dynamics of G^* and T^* plays out over the full 30 seconds and drives the eHA concentration below baseline. This autoreceptor model will be used for H_3 receptors on serotonin varicosities in Section 5. Full details of this histamine model can be found in [12].

5. The new serotonin model

In 2010, three of the authors (JB, HFN, MCR) created a mathematical model of serotonin synthesis in varicosities, storage in vesicles, release into the extracellular space, reuptake by serotonin transporters (SERTs), and control by serotonin

autoreceptors [5]. In subsequent years, they used the model to study and evaluate various hypotheses about serotonergic function including connections with dopaminergic signaling [8, 30], bursts in the DRN [31], the effects of serotonin on levodopa therapy [9], and serotonin dynamics in the basal ganglia [7]. In 2013, they began the collaboration with Parastoo Hashemi, which led to new insights into serotonergic function [11, 24, 32]. As discussed in Section 3, the experimental results in [11] and later papers revealed that various aspects of the 2010 model were naive and too simplistic. So, in 2020, the authors and collaborators expanded and revised the original model to take account of the new findings that we had learned [13]. Here we will briefly discuss the changes and some of the new results. A schematic diagram of the new model is in **Figure 6**.

In the experiments in the Hashemi Lab, the MFB is stimulated for 2 seconds and the antidromic spikes excite the DRN. The DRN sends bursts of action potentials to projection regions such as the SNr, the pre-frontal cortex (PFC), and the hippocampus. Serotonin rises rapidly in the extracellular space in the projection regions and then typically plunges substantially below basal levels within 30 seconds [11, 13, 33–35]. This almost certainly is because inhibition of release by the autoreceptors continues well after the serotonin concentration in the extracellular space has returned to basal levels. In our 2010 model, extracellular serotonin instantaneously affected release, and the Hashemi experiments showed that this is wrong. Therefore, in our new model [13] we include a biochemical model of the

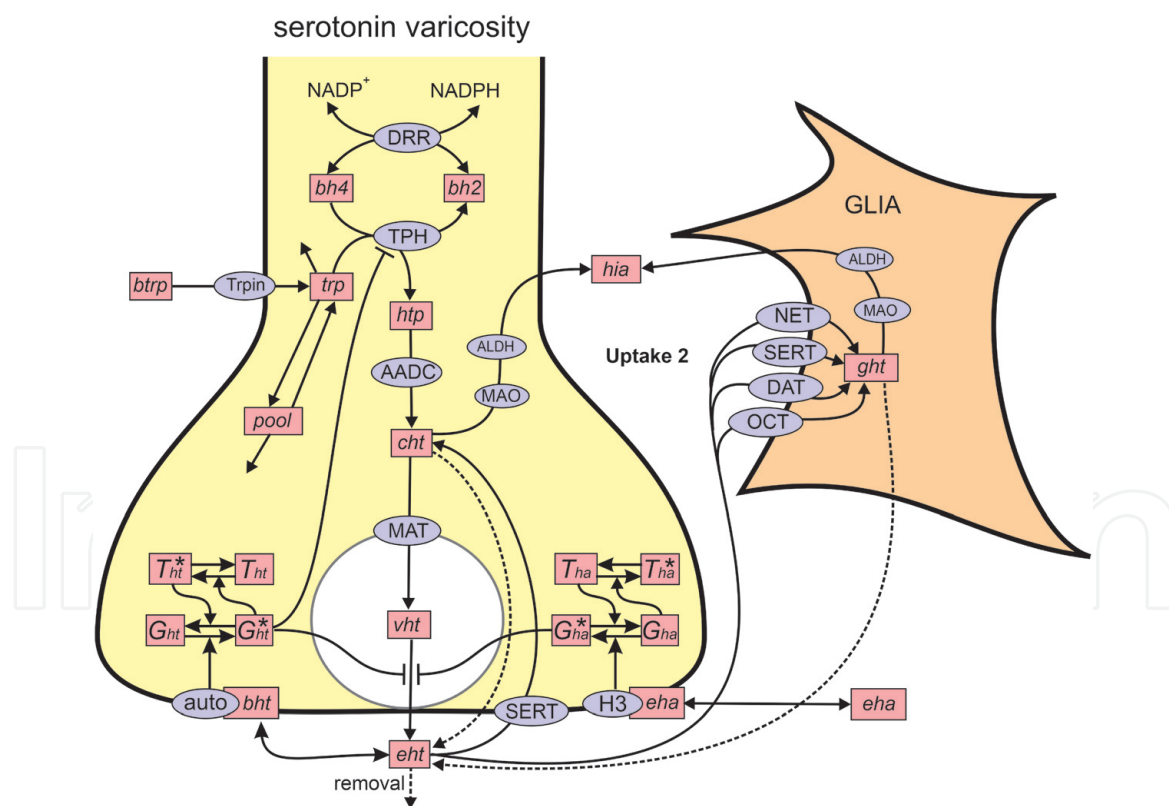


Figure 6.

Schematic diagram of the model. The rectangular boxes indicate substrates and blue ellipses contain the acronyms of enzymes or transporters. The names of the most important substrates are: Btrp, blood tryptophan; trp, cytosolic tryptophan; htp, 5-hydroxytryptamine; cht, cytosolic serotonin; vht, vesicular serotonin; eht, extracellular serotonin; hia, 5-hydroxyindoleacetic acid; ght, glial serotonin; eha, extracellular histamine. Names of enzymes and transporters are as follows: Trpin, neutral amino acid transporter; DRR, dihydrobiopterin reductase; TPH, tryptophan hydroxylase; AADC, aromatic amino acid decarboxylase; MAT, vesicular monoamine transporter; SERT, 5-HT_{1B} reuptake transporter; auto, 5-HT_{1B} autoreceptors; MAO, monoamine oxidase; ALDH, aldehyde dehydrogenase; NET, norepinephrine transporter; DAT, dopamine transporter; OCT, organic cation transporter. Removal means uptake by capillaries or diffusion out of the system.

cellular dynamics caused by serotonin binding to the autoreceptor, including activated receptor G-proteins and activated regulators of G-proteins. This autoreceptor model is similar to the histamine autoreceptor model discussed in Section 4. In addition, we showed in [24, 36] that histamine in the extracellular space inhibits the release of serotonin from serotonin varicosities. Therefore, in the new model, we also include a biochemical model of a histamine H₃ receptor on the serotonin varicosity that changes the dynamics of serotonin release. Both of these biochemical models for receptors are indicated schematically in **Figure 6**. As described in Section 3, in [11] we also showed that there are two different serotonin uptake mechanisms, SERTs that pump serotonin back into the varicosities and another uptake, which we call Uptake 2, that pumps serotonin into glial cells [16, 18, 37]. The kinetics of the two uptakes are quite different and both are included in our new model. We also include the effects of serotonin binding protein (SBP) that binds serotonin tightly in vesicles but releases it quickly when the vesicles open to the extracellular space. We also include leakage of 5-HT from the cytosol of neurons and glial cells into the extracellular space (dashed lines). All details of these changes and the full mathematical model can be found in [13]. We discuss below our new model for release from the vesicles. We also made a systems population model from our deterministic model and will show below how we used it to investigate certain aspects of the serotonin system.

In our model there is a constant basal rate of serotonin release at steady state. The question is how should we model release during the Hashemi Lab experiments where the MFB is stimulated for two seconds? In our previous work using the 2010 model we simply increased the firing rate for the two seconds of stimulation and then dropped it back to the basal rate. This issue is complicated by the existence of serotonin binding protein (SBP) that is attached to the inner wall of vesicles and binds serotonin tightly [38, 39]. We will assume that the dissociation is a first order reaction



If we start with one unit (nM) of SBP-serotonin being released into the extracellular space at time zero, then $SBP(t) = e^{-bt}$ and $\text{serotonin}(t) = 1 - e^{-bt}$. The rate of release of serotonin is the derivative, be^{-bt} . However, we are stimulating for two seconds, so SBP-serotonin complexes are continuously released into the extracellular space between $t = 0$ and $t = 2$ seconds. Assume that the rate of release is 1 nM/sec, so in two seconds, 2 nM of the complex are released. What is the rate of appearance, $R(t)$, of free serotonin for $t \leq 2$ and $t > 2$?

$$R(t) = \int_0^t \chi_{[s,2]} be^{-b(t-s)} ds \quad \text{for } t \leq 2, \quad (3)$$

and

$$R(t) = \int_0^2 \chi_{[s,2]} be^{-b(t-s)} ds \quad \text{for } t > 2. \quad (4)$$

Here $\chi_{[s,2]}$ is the function that is 1 on the interval $[s, 2]$ and zero otherwise. A straightforward calculation shows that:

$$R(t) = \begin{cases} 1 - e^{-bt} & \text{if } t \leq 2, \\ e^{-b(t-2)} - e^{-bt} & \text{if } t > 2. \end{cases} \quad (5)$$

Thus, for a two second stimulation, the rate of release will be proportional to $\text{fire}(t) = \text{basal rate} + r \cdot R(t)$ where r is the strength of the stimulation. Unfortunately, the dissociation constant b (inverse seconds) is not known, but we think it is in the range $0.5 \leq b \leq 2$ from our simulations of the Hashemi data, so we take $b = 1$ as our baseline case. The release of serotonin into the extracellular space will also be proportional to vht and it will also depend on the inhibition from the serotonin autoreceptors and the histamine H₃ receptor. Thus, overall release as a function of time will be

$$\text{inhib}_{ht}(G_{ht}^*) \cdot \text{inhib}_{ha}(G_{ha}^*) \cdot (\text{basal rate} + r \cdot R(t)) \cdot vht. \quad (6)$$

One of the first things that we did with our new model was to return to the 2014 data [11] that we discussed in Section 3 to see if our new serotonin model could easily match the average curves of fast, slow, and hybrid in the SNr, with relatively few, understandable changes of parameters. The experimental curves for fast, slow, and hybrid (**Figure 2**) do not look like typical response curves measured in the Hashemi Lab. For example, **Figure 7** shows an average of 17 male responses in the CA2 region of the hippocampus. Typical response curves peak, descend towards baseline, drop below baseline, and then curve back towards baseline, whereas the experimental curves in **Figure 2** keep descending. In thinking about this, we remembered that when the MFB is stimulated not only is 5-HT released in the SNr but histamine is also released. So we were in a good position to see if our new serotonin model, with its H₃ receptor, would allow us to match the 2014 SNr data. Unfortunately, we do not have the time course of histamine in the SNr in those experiments, because in 2014 the Hashemi Lab had not yet optimized the techniques to simultaneously measure 5-HT and histamine *in vivo* [24, 36]. So we will take our histamine time course in the extracellular space, *eha*, from the control and model curves in **Figure 5** of [12]. Note how complicated the dynamics of *eht* are. When one stimulates the MFB, serotonin is released into the extracellular space stimulating dynamical changes in the 5-HT_{1B} autoreceptor variables, B_{ht} , G_{ht}^* , T_{ht}^* . However, histamine also increases in the extracellular space stimulating dynamical changes in the H₃ receptor variables, B_{ha} , G_{ha}^* , T_{ha}^* . Both of the activated G-proteins, G_{ht}^* and G_{ha}^* inhibit serotonin release via the functions $\text{inhib}(G_{ht}^*)$ and $\text{inhib}_{ha}(G_{ha}^*)$.

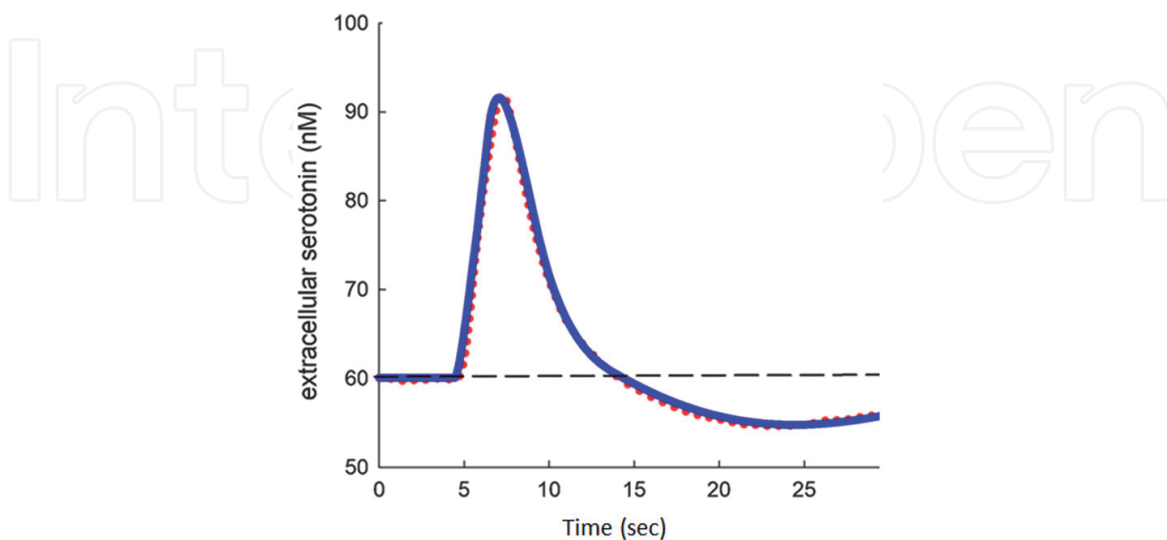


Figure 7.

Typical 5-HT response curves. The red dots show the average response of 23 male mice in the CA2 after stimulation of the MFB. The blue curve shows the average response predicted by the new 5-HT model. 5-HT rises rapidly and then descends rapidly as it is taken up by SERTs and Uptake 2. The concentration descend below baseline and then curve back towards baseline. This is the long-lasting autoreceptor effect. The average curve is simple and easy to interpret, but the individual curves show great variation; see **Figure 8**.

Furthermore, Uptake 2 is rapid but it probably also depends on the distance of glial cells from the electrodes in the three cases. Nevertheless, it was surprisingly easy to give adjustments for a small number of parameters that distinguish between fast, slow, and hybrid responses (see Figure 5 and Table 5 in [13]). The parameters that we had to change were the V_{max} of Uptake 2, the cutoff for Uptake 2, the strength of the inhibition by the 5-HT_{1B} and H₃ receptors, and the strength of firing during stimulation (r). It is completely reasonable that these parameters would be different for different electrode placements and different densities of receptors on the neuron. No other parameters were changed.

The model we have been discussing is a differential equations model (ODE); there is one differential equation for each of the pink boxed variables in **Figure 6**. All individuals, whether mouse or human, are different, and the variation is important for understanding experimental results and for precision medicine. We investigate this biological variation by creating a systems population model of the deterministic model given above. It is known that the expression levels of most enzymes can vary by about 25% or more between individuals [1–3]. Therefore, to create a systems population model, we choose new V_{max} values for each (or a subset) of the enzymes and transporters in **Figure 6** by selecting independently from a uniform distribution between 75% and 125% of the normal value. We then run the model to steady state and record all the concentrations and velocities. That is one virtual person (or mouse). If we do this 1000 times, we obtain a database of virtual individuals that we can analyze using the usual statistical tools. The difference is that all of these individuals have the same set of differential equations; only the coefficients are different. So we can experiment with the model to find the mechanistic reasons for particular statistical phenomena. We will give several examples that show why this approach is useful.

The steady state of *eht* in the ODE model is 60 nM; this should be thought of as the steady state for an average mouse (or an “average” person). We allowed the V_{max} values of TRPin, TPH, AADC, MAT, MAO, Uptake 2, and SERT to vary by 25% above and below their normal values independently. In addition, we allowed *fire(t)* to vary 25% above and below its normal value and we vary the strength of the 5-HT_{1B} autoreceptors similarly. Distributions of *eht* in various cases are shown in **Figure 9**. The green bars in Panel B show the distribution of *eht* values with normal tryptophan in the blood. The green bars are similar to distributions measured in the Hashemi Lab. The whole distribution moves left (the yellow bars in Panel B) if blood tryptophan is lowered from its normal values of 96 μM to 50 μM. In Panel A, we show what the distribution of *eht* would look like with no autoreceptors (orange bars) or autoreceptors that are twice strong. Thus, the systems population model allows one to see the effects of changes on a whole population, not just on an individual. Further, if the underlying ODE model is a good representation of the real physiology, then the variation in the population model should correspond to what is seen in the Lab. This gives another way of testing the validity of the underlying ODE model.

In [13] we used the ODE model to fit the average response curves for male and female mice in the hippocampus. Here we want to discuss the variation in the response curves. Panel A of **Figure 8** shows the responses of the 17 male mice. The experimental responses are measured and graphed for each mouse relative to the baseline level of *eht* that is represented in Panel A by *eht* = 0. One can see how large the variation is. The curves peak at different times and at different heights. Most, but not all, of the curves descend below baseline and their shapes are quite different; some continue descending while others reach a minimum and then rebound towards zero. The thick red curve is the mean and the thick black curve is the standard deviation, which is substantial even between 15 seconds and 30 seconds although the stimulation was only between t = 5 sec and t = 7 sec.

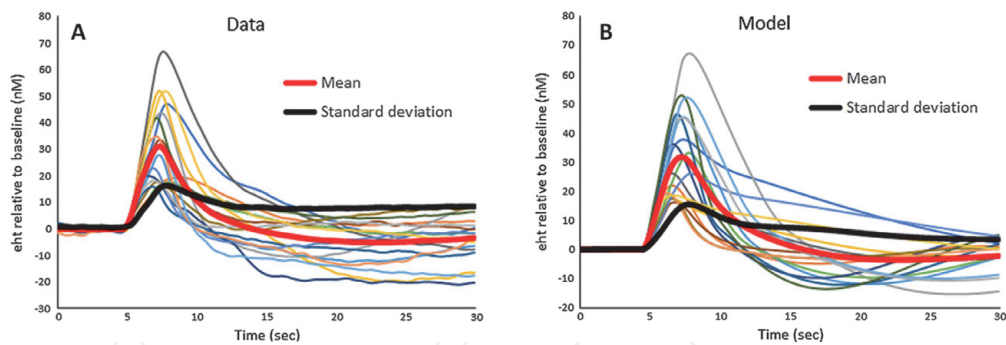


Figure 8.

Individual response curves. Panel A shows the time courses of eht in the hippocampus of 17 male mice after two seconds of stimulation at $t = 5$ seconds (Hashemi lab). The thick red and black curves are the time courses of the mean and standard deviation, respectively. The response curve are diverse and have different heights, peaks and shapes. Panel B shows 17 randomly selected response curves in a systems population model of 1000 individuals. The red and black curves are the time courses of the mean and the standard deviation of the 1000 model individuals, respectively. In both the experiments and the model, most (but not all) curves descend below baseline after peaking and then curve up towards the baseline. The mean curves and standard deviation curves are similar in the experiments and in the system population model.

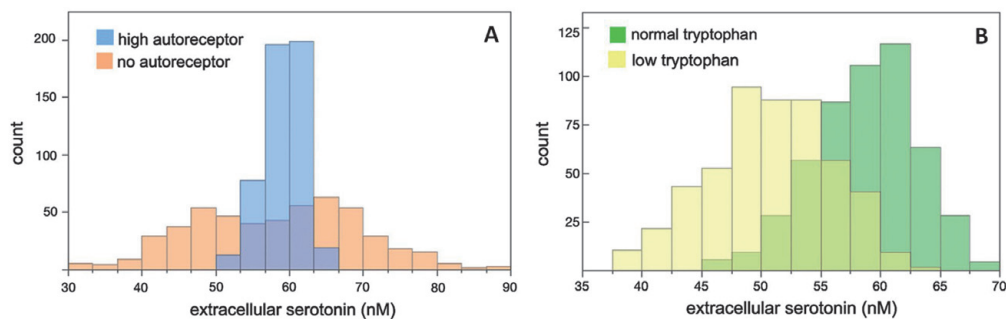
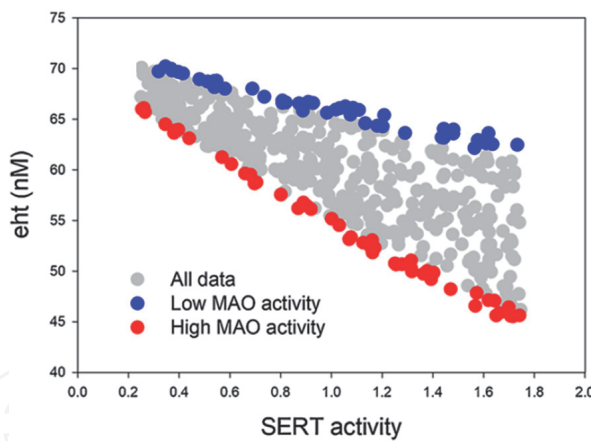


Figure 9.

Distributions of extracellular serotonin. Panel A shows the distribution of eht if there is no autoreceptor effect (pink bars) or if the autoreceptor effect is twice as strong as normal (blue bars). The green bars in panel B show the distribution of eht if the autoreceptor effect is “normal”. The green bars are similar to distributions measured in the Hashemi lab. The yellow bars in panel B show the distribution of eht if blood tryptophan is lowered from its normal value of $96\mu\text{M}$ to $50\mu\text{M}$. the distribution of eht moves substantially lower.

We investigated what variation in the main parameters of the model would be necessary to obtain the variation seen in the experiments. To do this we created a virtual population of 1000 individuals. The following parameters were varied uniformly from 40% below to 40% above their normal values: the V_{max} values for V_{AADC} , V_{CATAB} , V_{MAT} , V_{SERT} , V_{TPH} , V_{U2} ; the slope of *inhib* and *inhibsyn*; *eha*, the concentration of histamine in the extracellular space, and β that controls the speed of the autoreceptors. In addition, we varied the parameter r in $\text{fire}(t)$ by 25% and the time of the peak by 20%. Panel B of Figure 8 shows a random sample of 17 of the 1000 model male curves. The thick red curve is the mean of the 1000 model curves and the thick black curve is the standard deviation. The mean curve matches the experimental mean curve very well. The model standard deviation curve is very close to the experimental standard deviation except that at long times (20 second to 30 seconds) it descends slightly while the experimental standard deviation remains constant. Overall, one can see visually that the 17 model curves and the 17 experimental curves look similar as groups of curves. For each of the 1000 individuals, we record their steady state values as well as the values of all of their parameters so we can use multi-linear regression to find which parameters contributed most to the variation in the response curves. At $t = 7\text{ sec}$ (roughly the time of the peak), the three variables that contributed most, in order, were the strength of $\text{fire}(t)$, the timing of the peak in $\text{fire}(t)$, and the V_{max} of the SERTs. At $t = 15\text{ sec}$ (when most of

**Figure 10.**

Variation of SERT and MAO activity. In the population model, we varied only SERT activity and MAO activity. Each dot is one virtual individual, and the coordinates of each point are the activity of SERT (normal = 1) and the steady state concentration of eHT. The blue dots are individuals that have very low MAO activity and the red dots have very high MAO activity. Blocking the SERTs (changing the activity) has a much greater effect on high MAO activity individuals than on low MAO activity individuals.

the curves have returned to near baseline), the three parameters that contributed most to the variation in response were the V_{max} of TPH, the speed of the autoreceptors, and the V_{max} of MAT.

The population model allows us to approach a quite difficult mathematical question that would be very useful for understanding the biology and possible treatments. Suppose one has two populations of mice, for example male and female or obese and not obese or depressed and not depressed. Each of the two populations will produce a large family of experimental responses and those families of curves may be quite different. How can one estimate which parameters in the model cause the difference in the families? This is a way of using the response eht curves to probe the differences inside the neurons.

The expression levels of most enzymes can vary by about 25% or more between individuals [1–3]. This means that the V_{max} values of all the enzymes and transporters in our model vary by at least 25% and that any population of individuals will express this diversity. This poses large issues for drug discovery and treatment because it means that different individuals will react very differently to drugs, as is well-known [40–42]. Here, we present a simple example that shows how to use variation in a small number of variables to investigate questions about drug efficacy. In **Figure 10** we show results from our systems population model where we varied only two constants, the expression level (V_{max}) of SERT and the expression level of MAO, from 25–175% of normal. Each dot is an individual in a population of 500. The y-axis is the concentration of eht , extracellular serotonin, and the x-axis is the expression level of SERT. The blue dots are the individuals with low MAO activity and the red dots are individuals with high MAO activity. The conclusion is clear. Blocking SERTs with an SSRI (equivalent to lowering the expression level) will have a much greater effect on individuals with high MAO activity than on individuals with low MAO activity. Therefore, the systems population model suggests that it is high MAO individuals that will benefit the most from an SSRI. This shows how population models can be used to target specific questions.

6. Real-time *in vivo* neurotransmitter measurement techniques

To better answer physiological questions of the brain, especially about mental illness, it is critical to measure brain chemistry, specifically neurotransmitters.

Measuring neurochemistry is very challenging because neurotransmission is dynamic, and the brain tissue is very delicate. The earliest brain analysis methods utilized brain biopsies that were homogenized, separated and analyzed via HPLC [43]. These methods are offline and give an overview of whole tissue content, but not dynamic transmission. Microdialysis revolutionized brain analysis by utilizing a probe implanted into the brain, perfused with artificial cerebrospinal fluid [44, 45]. At the distal end of the probe is a semi-permeable membrane with a cut-off point such that analytes of interest can diffuse into the probe down a concentration gradient. The outgoing fluid, the dialysate, is collected and analyzed with a secondary method such as HPLC. The time resolution of this method is typically tens of minutes. Niche, electrochemical methods, such as fast scan cyclic voltammetry (FSCV) and fast scan-controlled adsorption voltammetry (FSCAV) can measure the subsecond temporal profile neurotransmission [33, 46, 47], outlined below.

6.1 Fast-scan cyclic voltammetry

Fast-Scan cyclic voltammetry is uniquely suited to measure neurotransmission *in vivo*. Its fast temporal dynamics allows for neurochemical detection on a subsecond timescale, approximately a thousand times faster than traditional cyclic voltammetry. Furthermore, FSCV measurements are performed at microelectrodes, typically carbon fiber microelectrodes (CFMEs). CFMEs have a small probe size (diameter 7 μm) and are biocompatible, creating minimal tissue damage and negligible immune response [48, 49]. Carbon electrodes also drive high sensitivity because their highly negative surface preconcentrates positively charged transmitters such as dopamine, serotonin, norepinephrine and histamine. These transmitters are then readily oxidized at the carbon surface, making it an ideal material for neurochemical measurements. Traditionally, FSCV has been utilized to measure dopamine [50–52]. However recent advances have allowed for the detection of other neurotransmitters, such as serotonin and histamine [24, 36, 53, 54].

Serotonin is measured using a CFME that has been modified by electropolymerization of a thin, uniform layer of Nafion. Nafion, a cation exchange polymer, increases the electrode sensitivity to serotonin while reducing the electrode poisoning effects of serotonin metabolites [54]. For *in vivo* experiments, this electrode is placed in the brain region of interest, such as the hippocampus, prefrontal cortex, or SNr. Because FSCV is a background subtracted technique, serotonin is evoked using an electrical stimulation placed in the MFB. Detection occurs by application of a waveform optimized for serotonin measurements. [12] This waveform has a resting potential of 0.2 V, scans up to 1.0 V, down to –0.1 V, and then back to the resting potential of 0.2 V at a scan rate of 1000 Vs^{-1} , applied at a frequency of 10 Hz. The signal is presented in the form of cyclic voltammograms (CVs) that qualify and quantify the substrate. **Figure 11** illustrates the FSCV experiment.

Histamine is particularly difficult to detect *in vivo* using FSCV because it lacks a clear, sharp oxidation peak. The Hashemi Lab developed a waveform that produces a unique electrochemical histamine signal. It has a resting potential of –0.5 V, scans to –0.7 V, up to 1.1 V, and then returns to the resting potential of –0.5 V at a scan rate of 600 Vs^{-1} . This waveform simultaneously detects serotonin and histamine release *in vivo* [24, 36].

6.2 Fast-scan controlled adsorption voltammetry

One limitation of FSCV is that because of the large capacitive current generated by the fast scan rate, it is a background subtracted technique [55]. This means that a

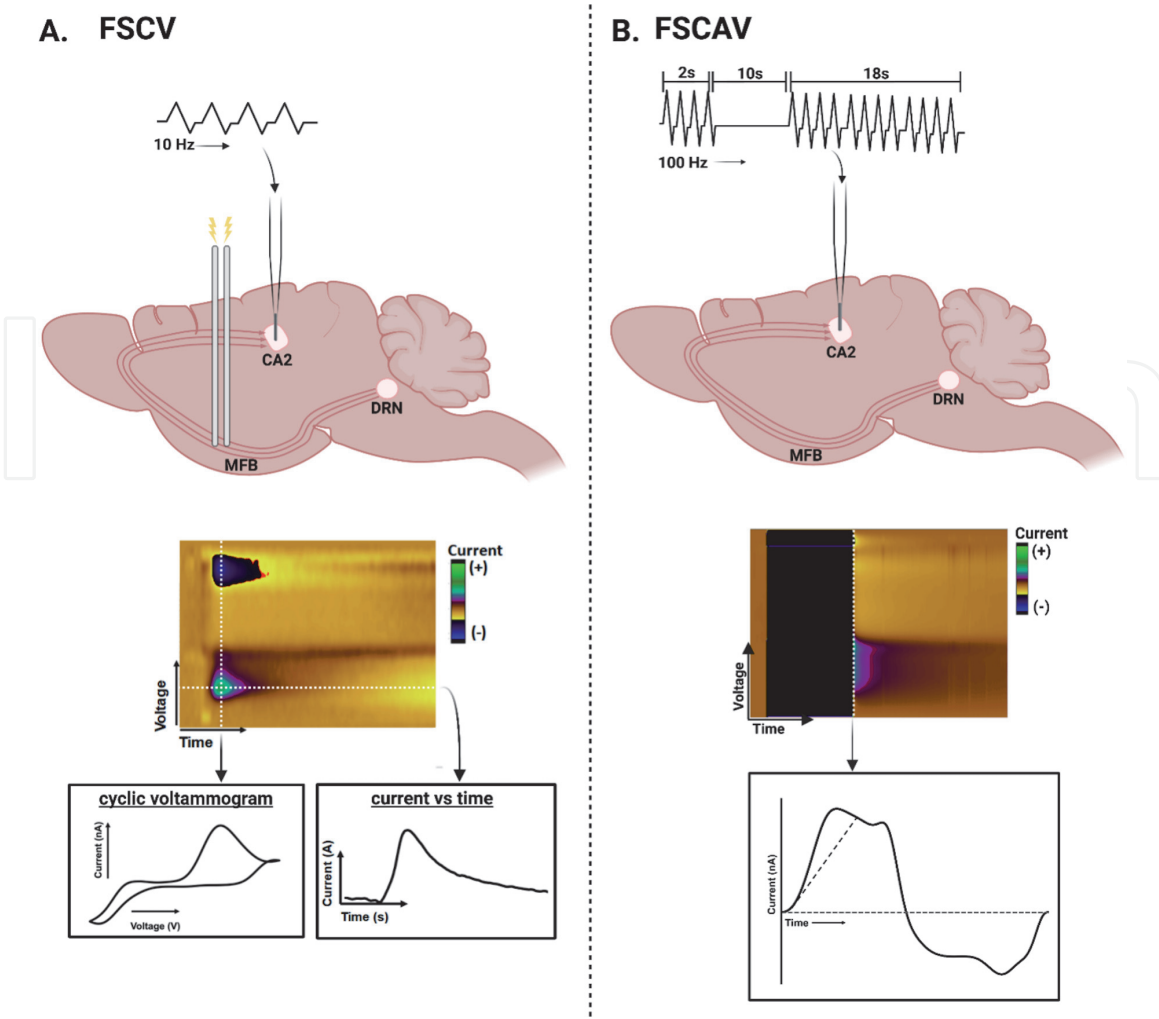


Figure 11.

Illustrative representation of an FSCV vs. FSCAV experiment described in-text. A. Shows the stimulation of the MFB to induce the release of serotonin in the CA2 and application of the serotonin waveform [53] to detect the evoked change in serotonin concentrations in the extracellular space over time. B. Depicts the modified waveform application for serotonin FSCAV [33] that negates the need for electrical stimulation to detect ambient concentrations of serotonin in the extracellular space each minute. This figure was created with Biorender.com.

change must be evoked, often electrically or pharmacologically. To address this issue, Atcherly et al. developed the method of fast-scan controlled adsorption voltammetry (FSCAV) to measure ambient concentrations of dopamine [56, 57]. This technique, illustrated in **Figure 11B**, was later adapted to measure serotonin [33]. FSCAV occurs at the same microelectrodes as FSCV. Serotonin FSCAV is performed in three steps: 1) The minimized adsorption step is implemented by applying the waveform at 100 Hz for 2 seconds. 2) The potential is held at +0.2 V for 10 sec for a period of controlled adsorption. 3) The waveform is reapplied at 100 Hz for 18 seconds. The CVs taken in the 3rd step are subtracted from the 1st step and thus serve as the ambient measurement.

7. The chemical basis of neuroinflammation

The vast majority of mental illnesses are associated with inflammation, especially depression which is highly comorbid with inflammation [58]. Increased levels of proinflammatory cytokines in the interleukin-1 and tumor necrosis factor families are linked to neuroinflammation [59, 60] across many different brain disorders. Chronic neuroinflammatory states have been implicated in neurodegenerative

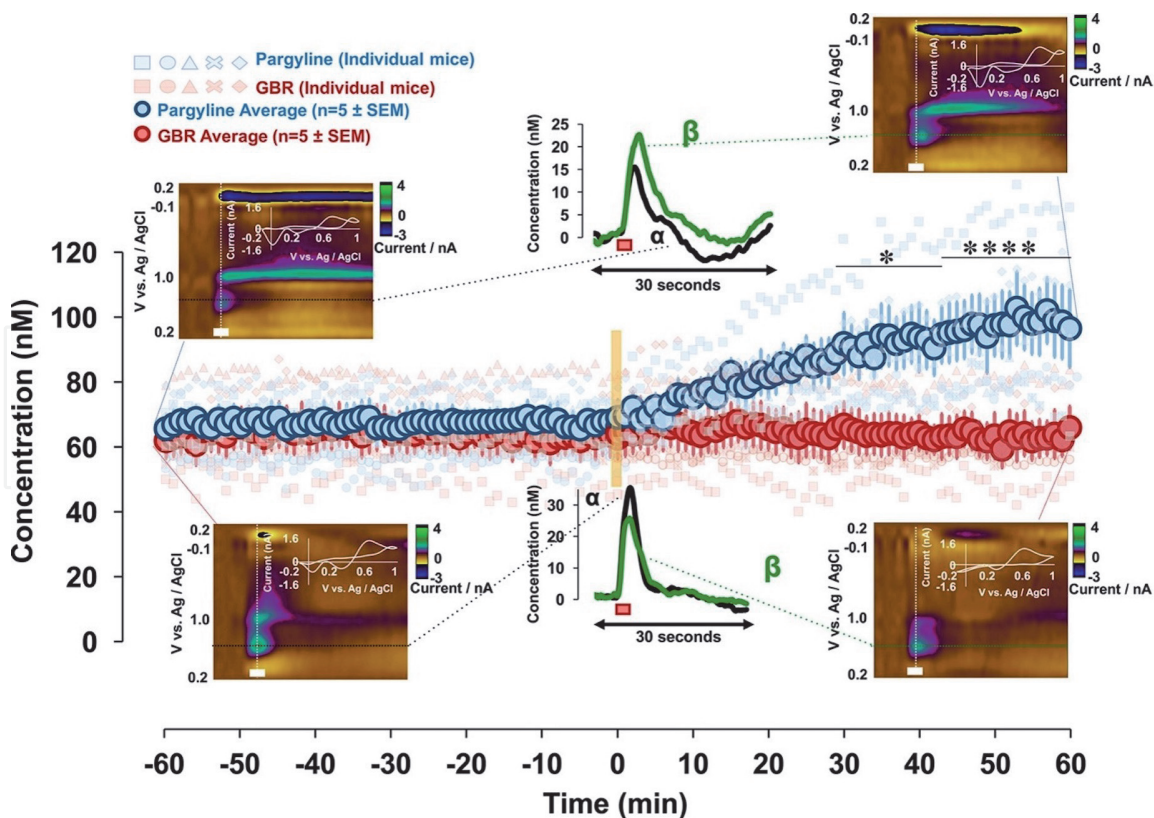
disorders such as Parkinson's Disease [61, 62], Alzheimer's Disease [63–65], and multiple sclerosis [66, 67], in addition to depression [58, 68] and bipolar disorder [69]. While these associations are clear, what is not known is the mechanism by which inflammation affects neurotransmission. We began to address this question by focusing on serotonin with FSCV and FSCAV. Serotonin is implicated in depression because the vast majority of antidepressants target the serotonin system [70]. Serotonin was first measured *in vivo* using FSCV in 1995 by Jackson et al. [53]. The authors detected serotonin in the rat striatum by forcing dopaminergic terminals to release serotonin following loading with 5-Hydroxytryptophan and dopamine depletion with α -methyl-p-tyrosine. More recently, using the same waveform we measured endogenous electrically evoked serotonin in the rat SNr [54]. Studies have since expanded to characterizing serotonin in different brain regions, studying differences in male and female mice, looking at serotonin and histamine co-modulation and observing the effects of inflammation on this co-modulation. We discuss our key findings below.

7.1 Serotonin dynamics in different brain regions

We first characterized evoked serotonin release and reuptake in the rat SNr following electrical MFB stimulation [54]. The SNr is of interest for serotonin detection as this area has the most dense serotonergic innervation in the brain and thus serotonin is the primary neurotransmitter released following electrical stimulation [71]. The signals obtained *in vivo* were pharmacologically verified using acute administration of the DAT inhibitor, GBR 12909, and the SSRI citalopram. The signals did not respond to DAT inhibition; however, following SERT inhibition, an increase in max amplitude and a slowing of the reuptake was observed. Serotonin response to varying doses of acute SSRI (1 mg kg^{-1} , 10 mg kg^{-1} , and 100 mg kg^{-1}) was examined [72], with uptake $t_{1/2}$ values increasing with dose concentration. However, no dose dependent trend was observed for max amplitude values. Further investigations of serotonin reuptake mechanisms [11] were performed by mathematical modeling through the development of a Michaelis–Menten kinetic model as previously described in Section 3. The presented model establishes a two uptake mechanism for serotonin, a notion that was described back in the 70s as Uptake 1 and 2 [16]. Uptake 1 refers to the high affinity, low efficiency system characterized by the serotonin transporters (SERTs) and Uptake 2 is serotonin clearance by the low affinity, high efficiency mechanism afforded by the dopamine, norepinephrine, organic cation, and plasma membrane transporters [16, 73].

While FSCV continues to provide insight into fast serotonin release and reuptake dynamics, it is limited by its inability to measure steady-state or ambient concentrations. To address this limitation, FSCAV was developed to detect absolute concentrations of both dopamine [57] and serotonin [33] *in vivo*. This technique (described above) yields fast, selective, and sensitive absolute concentrations of serotonin. Using FSCAV we reported serotonin concentrations of $64.9 \pm 2.3 \text{ nM}$ in the CA2 [33]. **Figure 12** shows ambient serotonin response to the monoamine oxidase B inhibitor, pargyline, in comparison to the DAT inhibitor, GBR 12909. Ambient serotonin levels increase following pargyline administration, but not following GBR administration, confirming that the signal is serotonin.

We expanded FSCV measurements of serotonin to the medial prefrontal cortex (mPFC) [32], another region associated with depression. Here, we found an interesting phenomenon whereby a double peak response was elicited in layers 1–3 of the mPFC. **Figure 13** shows examples of a single peak response as well as a variety of double peak responses in this brain region. Interestingly, each discrete peak had its own specific reuptake profile, thus we hypothesized that distinct axonal bundles in

**Figure 12.**

The dark blue markers represent the average response before and after pargyline (75 mg/kg, intra-peritoneal (*i.p.*)) administration and the dark red markers represent the average response before and after administration of GBR 12909 (15 mg/kg, *i.p.*). drug injection time is denoted by the yellow bar at 0 min. Representative colorplots, CVs, and concentration vs. time curves are inset (top, pargyline; bottom, GBR 12909, α = predrug and β = postdrug). (asterisks above blue markers indicate post hoc test: $*p < 0.0001$.) reprinted with permission from the American Chemical Society.

the MFB terminate in layer-dependent mPFC domains with specific uptake transporters. A mathematical model confirmed that the double peaks could be explained by diffusion of neurotransmitter to the electrode from two different sources, one close and one further away.

Finally, in this part of our work, we compared the *in vivo* serotonin signals between the SNr, the CA2 region of the hippocampus, and the mPFC [35]. We found that the different responses could be modeled as a function of the percentage of Uptake 1/Uptake 2 transporters with the model predicting the largest concentration of serotonin transporters in the SNr. We verified this notion with confocal microscopy and concluded that FSCV could be a potentially useful tool for chemical imaging of local cytoarchitecture. Interestingly, and counterintuitively, the SNr, with the highest density of serotonin terminals and axons, had the lowest ambient levels of serotonin. We realized that this was because of the high affinity of SERTs (Uptake 1 transporters) in this region that serve to maintain steady state levels lower than the other two regions with fewer SERTs.

7.2 Serotonin dynamics between the sexes

The prevalence of depression differs between males and females, with women being more likely to suffer from the disorder than men [74–76]. As such, it is important to investigate neurochemical and pharmacodynamic disparities across the sexes. In the hippocampus, we observed no significant differences in the evoked serotonin maximum amplitude or the $t_{1/2}$ of clearance between male and female mice [34]. Furthermore, no differences were detected between the mean signal and

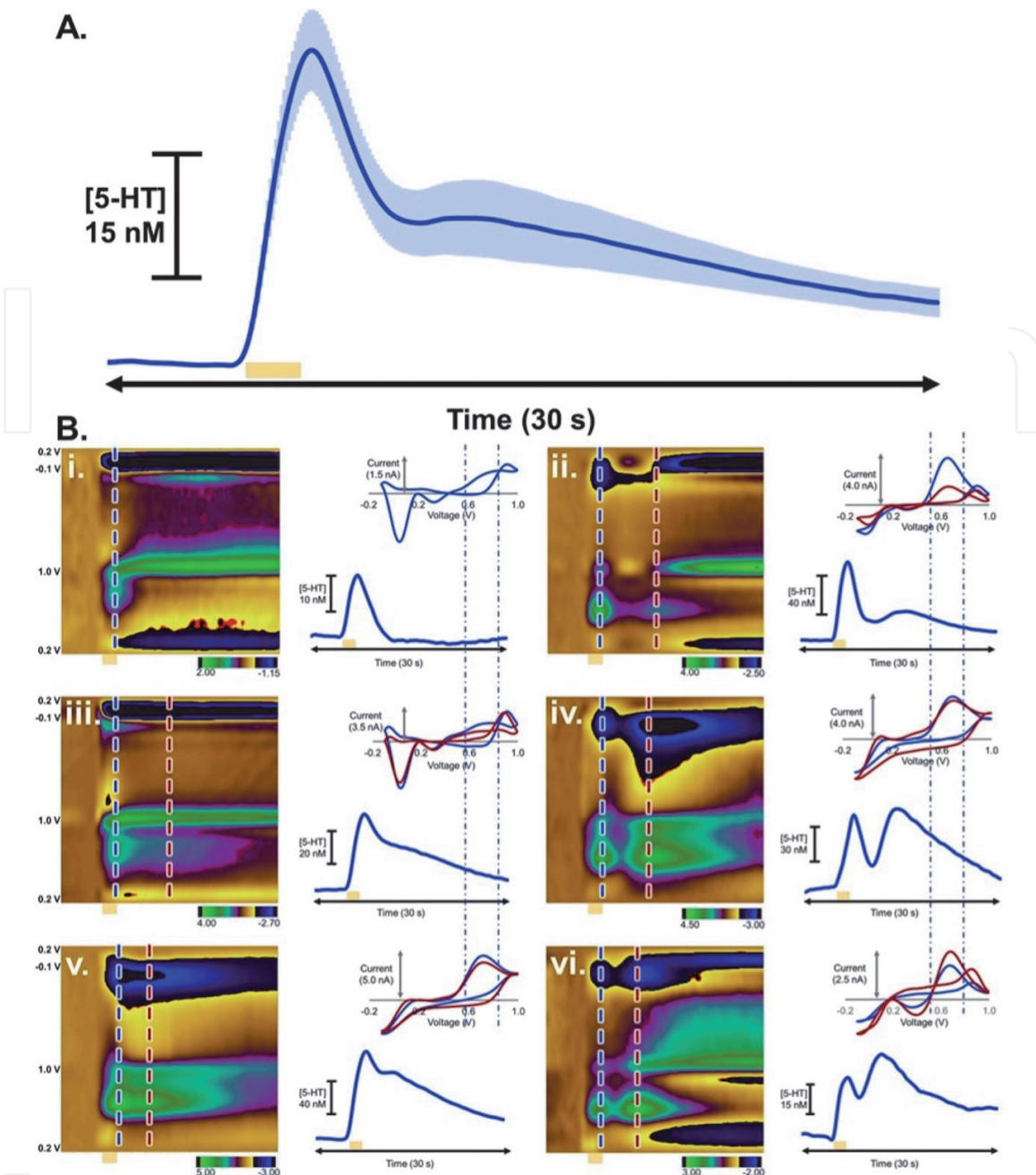


Figure 13. Representation of single and double peaks reported by West et al. 2019 in the mPFC. The average serotonin response is depicted in (A). Varying signals are shown in (B) with a traditional single peak displayed in (i.) and five of the most common types of double peaks shown in (ii.-vi.). The inset contains the CVs of both peaks. The first peak is shown in blue and the second in red. Reprinted with permission from Elsevier.

the signal in different stages of the female mouse estrous cycle. This suggests that there are no major sex differences in the release or reuptake machinery in drug naïve mice. Likewise, no significant differences were detected across sexes in ambient levels of serotonin using FSCAV. Differences in clinical efficacy have been observed following the administration of SSRIs, a class of commonly prescribed antidepressants [77]. Following acute administration of the SSRI, escitalopram, ambient serotonin concentrations increased significantly, however no differences were seen between male and female mice. On the other hand, differences were observed in the evoked serotonin reuptake decay curve. At all four doses given (1, 3, 10 and 30 mg/kg) the female mice had a lower percent change in reuptake compared to the males. We speculated that in female mice, compensatory mechanisms (likely via autoreceptors) exist to counteract hormone-mediated chemical fluxes that may affect serotonin.

7.3 Histaminergic transmission and modulation of serotonin

As outlined above, inflammation (peripheral and brain) is becoming synonymous with the pathophysiology of depression [58]. The monoamine histamine is a major inflammatory mediator in the body [77], associated with allergic reactions. However, less is known about histamine's role in the brain. While traditionally believed to be a neuromodulator in the CNS, recent studies have implicated histamine in neuroinflammatory processes as well [78, 79]. To study fast histaminergic dynamics, we optimized an FSCV waveform to simultaneously detect histamine and serotonin *in vivo* [24, 36]. Histamine oxidation was pharmacologically validated in the posterior hypothalamus following application of tacrine, a histamine N-methyltransferase inhibitor, and thioperamide, an H₃ receptor antagonist. Acute tacrine administration slowed the reuptake of histamine significantly, while thioperamide slowed the reuptake and increased the max amplitude. Upon electrochemical release of histamine, a rapid inhibition of serotonin is observed as shown in **Figure 3**. In this figure, release and reuptake of histamine (a) and serotonin (b) are shown before and after thioperamide (H₃ receptor antagonist) administration, where the dots are the result of a simple mathematical model where the receptor and autoreceptor strengths were changed dynamically by hand. Using the new full histamine and serotonin models (Sections 4 and 5) with the chemistry of the autoreceptors and the H₃ receptors, we were able to predict the experimental results just by using the release and reuptake curve for histamine in the extracellular space that we previously measured.

7.4 Serotonin and histamine in inflammation models

The inhibition of serotonin by histamine fueled our interest in the co-modulation of these analytes in inflammation models. In recent work, we found that upon acute lipopolysaccharide (LPS) induced inflammation, ambient serotonin levels rapidly decreased as a function of increased histamine. Escitalopram was much less capable of increasing the serotonin levels under this inflammation state. We found that this was because escitalopram (and other common antidepressants) inhibit histamine reuptake. This inhibition raises histamine, which depresses serotonin release, counteracting the effect of the antidepressant on the SERTs. Only with the dual strategy of inhibiting serotonin reuptake (by an SSRI) and inhibiting histamine synthesis were we able to return the serotonin to pre-inflammation control levels. We are now actively studying serotonin/histamine co-modulation in other inflammation/depression models in mice including chronic stress and neurodegeneration.

8. Future outlook

Our *in vivo* studies have allowed us to measure and compare and contrast serotonin in different brain regions, to study serotonin dynamics in male and female mice, to investigate serotonin and histamine co-modulation and to ask how this modulation changes under inflammation. This program has provided invaluable information about the dynamics of these two modulators in health and pathophysiology in mice. Our future goals are to apply our findings to *ex vivo* models that more closely mimic human inflammation as a path towards depression diagnosis and treatment. We are exploring a variety of stem cell models, derived from humans, as model systems for personalized diagnostic and drug screening platforms. The continuing, active collaboration and innovation between the

experimentalists and the mathematical modelers, as has been the case in the last seven years, will drive novel discoveries in our future program.

Acknowledgements

The authors would like to thank Brenna Park for helpful edits and making **Figure 11**. Partial support for this research came from NIH through R01MH106563-01A1 (PH, JB, HFN, MCR) and 1R21MH109959-01A1 (PH, JB, HFN, MCR) and from the NSF through support for the Mathematical Biosciences Institute, DMS-1440386.

Abbreviations

5-HT	Serotonin
CFME	Carbon fiber microelectrode
CV	Cyclic voltammograms
DA	Dopamine
DAT	Dopamine transporter
DRN	Dorsal raphe nucleus
FSCV	Fast-scan cyclic voltammetry
FSCAV	Fast-scan controlled adsorption voltammetry
TH	Tyrosine hydroxylase
TPH	Tryptophan hydroxylase
MAO	Monoamine oxidase
MFB	Medial forebrain bundle
ODE	Ordinary differential equation
PFC	Prefrontal cortex
RGS	Regulator of G-protein signaling
SBP	Serotonin binding protein
SERT	Serotonin transporter
SNr	Substantia nigra pars reticulata [
SSRI	Selective serotonin reuptake inhibitor



Author details

Janet Best^{1*†}, Anna Marie Buchanan^{2†}, Herman Frederik Nijhout³, Parastoo Hashemi^{2,4} and Michael C. Reed³

1 The Ohio State University, Columbus, OH, USA

2 University of South Carolina, Columbia, SC, USA

3 Duke University, Durham, NC, USA

4 Imperial College, London, UK

*Address all correspondence to: best.82@osu.edu

† These authors contributed equally.

IntechOpen

© 2021 The Author(s). Licensee IntechOpen. This chapter is distributed under the terms of the Creative Commons Attribution License (<http://creativecommons.org/licenses/by/3.0>), which permits unrestricted use, distribution, and reproduction in any medium, provided the original work is properly cited. CC BY

References

- [1] Oleksiak, M., Churchgill, G., Crawford, D.: Variation in gene expression within and among natural populations. *Nat. Genetics* **32**, 261–266 (2002)
- [2] Boeuf, S., Keijer, J., Hal, N., Klaus, S.: Individual variation of adipose gene expression and identification of covariated genes by cdna microarrays. *Physiol. Genomics* **11**, 31–36 (2002)
- [3] Sigal, A., Milo, R., Chen, A., Gava-Zatorsky, N., Klein, Y., Liron, Y., Rosenfeld, N., Danon, T., Perzov, N., Alon, U.: Variability and memory of protein levels in human cells. *Nature letters* **444**, 643–646 (2006)
- [4] Best, J.A., Nijhout, H.F., Reed, M.C.: Homeostatic mechanisms in dopamine synthesis and release: a mathematical model. *Theor Biol Med Model* **6**, 21 (2009)
- [5] Best, J.A., Nijhout, H.F., Reed, M.C.: Serotonin synthesis, release and reuptake in terminals: a mathematical model. *Theor Biol Med Model* **7**, 34 (2010)
- [6] Reed, M.C., Best, J.A., Nijhout, H.F.: Passive and active stabilization of dopamine in the striatum. *BioScience Hypotheses* **2**, 240–244 (2009)
- [7] Reed, M., Nijhout, H.F., Best, J.: Computational studies of the role of serotonin in the basal ganglia. *Frontiers Integrative Neuroscience* **7**, 1–8 (2013)
- [8] Best, J., Oakley, G., Reed, M., Nijhout, H.F.: Mathematical Models: Interactions between serotonin and dopamine in Parkinson's disease. In: Rana, A.Q. (ed.) *Etiology and Pathophysiology of Parkinson's Disease*. InTech, London, UK (2011)
- [9] Reed, M., Nijhout, H.F., Best, J.: Mathematical insights into the effects of levodopa. *Frontiers Integrative Neuroscience* **6**, 1–24 (2012)
- [10] Hashemi, P., Dankowski, E., Wood, K., Ambrose, R., Wightman, R.: In vivo electrochemical evidence for simultaneous 5-HT and histamine release in the rat substantia nigra pars reticulata following medial forebrain bundle stimulation. *J. Neurochem.* **118**, 749–759 (2011)
- [11] Wood, K.M., Zeqja, A., Nijhout, H.F., Reed, M.C., Best, J.A., Hashemi, P.: Voltammetric and mathematical evidence for dual transport mediation of serotonin clearance in vivo. *J. Neurochem.* **130**, 351–359 (2014)
- [12] Best, J., Nijhout, H.F., Samaranayake, S., Hashemi, P., Reed, M.: A mathematical model for histamine synthesis, release, and control in varicosities. *Theoretical Biology and Medical Modelling* **14**, 24 (2017)
- [13] Best, J., Duncan, W., Sadre-Marandi, F., Nijhout, H.F., Reed, M.: Autoreceptor control of serotonin dynamics. *BMC Neuroscience*, 1–20 (2020)
- [14] Knappskog, P., Flatmark, T., Mallet, J., Lüdecke, B., Bartholomé, K.: Recessively inherited L-DOPA-responsive dystonia caused by a point mutation (Q381K) in the tyrosine hydroxylase gene. *Hum. Mol. Genet.* **4**, 1209–1212 (1995)
- [15] Bunin, M., Prioleau, C., Mailman, R., Wightman, R.: Release and uptake rates of 5-hydroxytryptamine in the dorsal raphe and substantia nigra of the rat brain. *J Neurochem* **70**, 1077–1087 (1998)
- [16] Shaskan, E., Snyder, S.: Kinetics of serotonin accumulation into slices from rat brain: relationship to catecholamine uptake. *J. Pharmacol. Exp. Ther.* **175**, 404–418 (1970)

- [17] Daws, L.C., Koek, W., Mitchell, N. C.: Revisiting serotonin reuptake inhibitors and the therapeutic effects of “uptake 2” in psychiatric disorders. *ACS Chem. Neurosci.* **4**, 16–21 (2013)
- [18] Horton, R., Apple, E., Owens, W.: Decynium-22 enhances ssri-induced antidepressant-like effects in mice: uncovering novel targets to treat depression. *J. Neurosci* **33**, 10534–10543 (2013)
- [19] Monachon, M.-A., Burkard, W.P., Jalfre, M., Haefely, W.: Blockade of central 5-hydroxytryptamine receptors by methiothepin. *Naunyn-Schmiedeberg's Arch Pharmacol* **274**, 192–197 (1972)
- [20] Haas, H., Sergeeva, O., Selbach, O.: Histamine in the nervous system. *Physiological Reviews* **88**, 1183–1241 (2008)
- [21] Schwartz, J.-C.: Histamine as a transmitter in brain. *Life Sciences* **17**, 503–518 (1974)
- [22] Maeyama, K., Watanabe, T., Yamatodani, A., Taguchi, Y., Kambe, H., Wada, H.: Effect of alpha-fluoromethylhistidine on the histamine content of the brain of w/wv mice devoid of mast cells: turnover of brain histamine. *J. Neurochem.* **41**, 128–134 (1983)
- [23] Feldman, R.S., Meyer, J.S., Quenzer, L.F.: *Principles of Neuropharmacology*. Sinauer Associates, Inc, Sunderland, MA. (1997)
- [24] Samaranayake, S., Abdalla, A., Robke, R., Nijhout, H.F., Reed, M., Best, J., Hashemi, P.: A voltammetric and mathematical analysis of histaminergic modulation of serotonin in the mouse hypothalamus. *J. Neurochem.* **138**, 374–383 (2016)
- [25] Annamalai, B., Varman, D.R., Horton, R.E., Daws, L.C., Jayanthi, L.D., Ramamoorthy, S.: Histamine receptors regulate the activity, surface expression, and phosphorylation of serotonin transporters. *ACS Chem. Neurosci.* **11**, 466–476 (2020)
- [26] Spaethling, J.M., Piel, D., Dueck, H., Buckley, P.T., Morris, J.F., Fisher, S.A., Lee, J., Sul, J.-Y., Kim, J., Bartfai, T., Beck, S.G., Eberwine, J.H.: Serotonergic neuron regulation informed by *in vivo* single-cell transcriptomics. *FASEB J* **28**, 771–780 (2014)
- [27] Bernaerts, P., Lamberty, Y., Tirelli, E.: Histamine H3 antagonist thioperamide dose-dependently enhances memory consolidation and reverses amnesia induced by dizocilpine or scopolamine in a one-trial inhibitory avoidance task in mice. *Behav. Brain Res.* **154**, 211–219 (2004)
- [28] Nieto-Alamilla, G., Márquez-Gómez, R., García-Gálvez, A., Morales-Figueroa, G., Arias-Montaño, J.: The histamine H3 receptor: structure, pharmacology, and function. *Mol Pharmacol* **90**, 649–673 (2016)
- [29] Willars, G.: Mammalian rgs proteins: multifunctional regulators of cellular signalling. *Seminars in Cell and Developmental Biology* **17**, 363–376 (2006)
- [30] Best, J.A., Nijhout, H.F., Reed, M.C.: Models of dopaminergic and serotonergic signaling. *Pharmacopsychiatry* **43**(Supp. 1), 561–566 (2010)
- [31] Best, J., Reed, M., Nijhout, H.F.: Bursts and the efficacy of selective serotonin reuptake inhibitors. *Pharmacopsychiatry* **44**(Supp1), 76–83 (2011)
- [32] West, A., Best, J., Abdalla, A., Nijhout, H.F., Reed, M., Hashemi, P.: Voltammetric evidence for discrete serotonin circuits, linked to specific reuptake domains, in the mouse medial

- prefrontal cortex. *Neurochem. Inter.* **123**, 50–58 (2019)
- [33] Abdalla, A., Atcherley, C., Pathirathna, P., Samaranayake, S., Qiang, B., Pena, E., Morgan, S., Heien, M., Hashemi, P.: In vivo ambient serotonin measurements at carbon-fiber microelectrodes. *Anal. Chem.* **89**, 9703 (2017)
- [34] Saylor, R., Hersey, M., West, A., Buchanan, A., Berger, S., Nijhout, H.F., Reed, M., Best, J., Hashemi, P.: In vivo hippocampal serotonin dynamics in male and female mice: Determining effects of acute escitalopram using fast scan cyclic voltammetry. *Frontiers Neurosci.* doi: [10.3389/fnins.2019.00362](https://doi.org/10.3389/fnins.2019.00362) (2019)
- [35] Abdalla, A., West, A., Jin, Y., Saylor, R., Qiang, B., Pena, E., Linden, D., Nijhout, H.F., Reed, M., Best, J., Hashemi, P.: Fast serotonin voltammetry as a versatile tool for mapping dynamic tissue architecture: I. responses at carbon fibers describe local tissue physiology. *J Neurochem* **153**, 33–50 (2020)
- [36] Samaranayake, S., Abdalla, A., Robke, R., Wood, K., Zeqja, A., Hashemi, P.: In vivo histamine voltammetry in the mouse premammillary nucleus. *Analyst* **140**, 3759–3765 (2015)
- [37] Daws, L., Koek, W., N.Mitchell: Revisiting serotonin reuptake inhibitors and the therapeutic potential of “uptake-2” in psychiatric disorders. *ACS Chem. Neurosci.* **4**, 16–21 (2013)
- [38] Gershon, M., Liu, K., Karpiak, S., Tamir, H.: Storage of serotonin in vivo as a complex with serotonin binding protein in central and peripheral serotonergic neurons. *J. Neurosci* **3**, 1901–1911 (1983)
- [39] Liu, K.-P., Gershon, M., Tamir, H.: Identification, purification, and characterization of two forms of serotonin binding protein from rat brain. *J. Neurochem.* **44**, 1289–1301 (1985)
- [40] Selim, K., Kaplowitz, N.: Hepatotoxicity of psychotropic drugs. *Hepatology* **29**, 1347–1351 (1999)
- [41] J, W., Weale, M., Smith, A., Gatriz, F., Fletcher, B., Thomas, M., Bradman, N., Goldstein, D.: Population genetic structure of variable drug response. *Nature Genetics* **29**, 265–269 (2001)
- [42] Cho, Y.-T., Yang, C.-W., Chu, C.-Y.: Drug reaction with eosinophilia and systemic symptoms (DRESS): An interplay among drugs, viruses, and immune system. *Int. J. Molecular Sciences* **18**, 1–21 (2017)
- [43] Vanhala, A., Yamatodani, A., Panula, P.: Distribution of histamine-, 5-hydroxytryptamine-, and tyrosine hydroxylase-immunoreactive neurons and nerve fibers in developing rat brain. *J Comp Neurol* **347**(1), 101–114 (1994)
- [44] Bito, L., Davson, H., Levin, E., Murray, M., Snider, N.: The concentrations of free amino acids and other electrolytes in cerebrospinal fluid, in vivo dialysate of brain, and blood plasma of the dog. *J Neurochem* **13**(11), 1057–1067 (1966)
- [45] Delgado, J.M.R., DeFeudis, F.V., Roth, R.H., Ryugo, D.K., Mitruka, B.M.: Dialytrode for long term intracerebral perfusion in awake monkeys. *Arch Int Pharmacodyn Ther* **198**(1), 9–21 (1972)
- [46] Robinson, D.L., Venton, J.M., Heien, M.L.A.V., Wightman, R.M.: Detecting subsecond dopamine release with fast-scan cyclic voltammetry in vivo. *Clinical Chemistry* **49**, 1763–1773 (2003)
- [47] Hersey, M., Berger, S.N., Holmes, J., West, A., Hashemi, P.: Recent developments in carbon sensors for at-

- source electroanalysis. *Anal. Chem.* **91** (1), 27–43 (2019)
- [48] Peters, J.L., Miner, L.H., Michael, A., Sesack, S.R.: Ultrastructure at carbon fiber microelectrode implantation sites after acute voltammetric measurements in the striatum of anesthetized rats. *J Neurosci Meth* **137**(1), 9–23 (2004)
- [49] Jaquins-Gerstl, A., Michael, A.C.: Comparison of the brain penetration injury associated with microdialysis and voltammetry. *J Neurosci Meth* **183**(2), 127–135 (2009)
- [50] Millar, J., Stamford, J.A., Kruk, Z.L., Wightman, R.M.: Electrochemical, pharmacological and electrophysiological evidence of rapid dopamine release and removal in the rat caudate nucleus following electrical stimulation of the median forebrain bundle. *European Journal of Pharmacol* **109**(3), 341–8 (1985)
- [51] Stamford, J.A., Kruk, Z.L., Millar, J., Wightman, R.M.: Striatal dopamine uptake in the rat: In vivo analysis by fast cyclic voltammetry. *Neurosci Lett* **51**(1), 133–138 (1984)
- [52] Yamamoto, B.K., Spanos, L.J.: The acute effects of methylenedioxymethamphetamine on dopamine release in the awake-behaving rat. *Eur J Pharmacol* **148**(2), 195–203 (1988)
- [53] Jackson, B., Dietz, S., Wightman, R.: Fast-scan cyclic voltammetry of 5-hydroxytryptamine. *Analytical Chemistry* **67**, 1115–1120 (1995)
- [54] Hashemi, P., Dankoski, E., Petrovic, J., Keithley, R., Wightman, R.: Voltammetric detection of 5-hydroxytryptamine release in the rat brain. *Analytical Chemistry* **81**, 9462 (2009)
- [55] Howell, J.O., Kuhr, W.G., Enzman, R.E., Wightman, R.M.: Background subtraction for rapid scan voltammetry. *J Electroanalytical Chemistry and Interfacial Electrochem* **209**(1), 77–90 (1986)
- [56] Atcherley, C.W., Laude, N.D., Parent, K.L., Heien, M.L.: Fast-scan controlled-adsorption voltammetry for the quantification of absolute concentrations and adsorption dynamics. *Langmuir* **29**(48), 14885–92 (2013)
- [57] Atcherley, C.W., Wood, K.M., Parent, K.L., Hashemi, P., Heien, M.L.: The coaction of tonic and phasic dopamine dynamics. *Chem. Commun.* **51**, 2235–2238 (2015)
- [58] Amodeo, G., Trusso, M., Fagiolini, A.: Depression and inflammation: Disentangling a clear yet complex and multifaceted link. *Neuropsychiatry (London)* **07**(4), 448–457 (2017)
- [59] Singhal, G., Jaehne, E.J., Corrigan, F., Toben, C., Baune, B.T.: Inflammasomes in neuroinflammation and changes in brain function: a focused review. *Front. Neurosci.* **8**(315) (2014)
- [60] Becher, B., Spath, S., Goverman, J.: Cytokine networks in neuroinflammation. *Nature Reviews Immunology* **17**(1), 49–59 (2017)
- [61] McGeer, E.G., McGeer, P.L.: The role of anti-inflammatory agents in parkinson's disease. *CNS Drugs* **21**(10), 789–797 (2007)
- [62] Nagatsu, T., Mogi, M., Ichinose, H., Togari, A.: Cytokines in Parkinson's disease. *J Neural Transmission Suppl* **58**, 143–151 (2000)
- [63] Swardfager, W., Lanctot, K., Rothenburg, L., Wong, A., Cappell, J., Herrmann, N.: A meta-analysis of cytokines in Alzheimer's disease. *Biol Psychiatry* **68**(10), 930–941 (2010)
- [64] Griffin, W.S., Stanley, L.C., Ling, C., White, L., MacLeod, V., Perrot, L.J.,

- 3rd, C.L.W., Araoz, C.: Brain interleukin 1 and S-100 immunoreactivity are elevated in Down syndrome and Alzheimer disease. *PNAS* **86**(19), 7611–7615 (1989)
- [65] Strauss, S., Bauer, J., Ganter, U., Jonas, U., Berger, M., Volk, B.: Detection of interleukin-6 and alpha 2-macroglobulin immunoreactivity in cortex and hippocampus of Alzheimer's disease patients. *Lab Invest* **66**(2), 223–230 (1992)
- [66] Palle, P., Monaghan, K.L., Milne, S.M., Wan, E.C.K.: Cytokine signaling in multiple sclerosis and its therapeutic applications. *Medical Sciences (Basel, Switzerland)* **5**(4), 23 (2017)
- [67] Chang, J.R., Zaczynska, E., Katsetos, C.D., Platsoucas, C.D., Oleszak, E.L.: Differential expression of TGF-beta, IL-2, and other cytokines in the CNS of theiler's murine encephalomyelitis virus-infected susceptible and resistant strains of mice. *Virology* **278**(2), 346–360 (2000)
- [68] Young, J.J., Bruno, D., Pomara, N.: A review of the relationship between proinflammatory cytokines and major depressive disorder. *Journal of Affective Disorders* **169**, 15–20 (2014)
- [69] Fries, G.R., Walss-Bass, C., Bauer, M.E., Teixeira, A.L.: Revisiting inflammation in bipolar disorder. *Pharmacology Biochemistry and Behavior* **177**, 12–19 (2019)
- [70] Mayo Clinic Staff: Selective Serotonin Reuptake Inhibitors (SSRIs). <https://www.mayoclinic.org/diseases-conditions/depression/in-depth/ssris/art-20044825>.
- [71] Cragg, S.J., Hawkey, C.R., Greenfield, S.A.: Comparison of serotonin and dopamine release in substantia nigra and ventral tegmental area: region and species differences. *J Neurochem* **69**(6), 2378–86 (1997)
- [72] Wood, K.M., Hashemi, P.: Fast-scan cyclic voltammetry analysis of dynamic serotonin responses to acute escitalopram. *ACS Chem. Neurosci.* **4**(5), 715–720 (2013)
- [73] Daws, L., Montenez, S., Owens, W., Gould, G., Frazer, A., Toney, G., Gerhardt, G.: Transport mechanisms governing serotonin clearance in vivo revealed by high speed chronoamperometry. *J Neurosci Meth* **143**, 49–62 (2005)
- [74] Weissman, M.M., Klerman, G.L.: Sex differences and the epidemiology of depression. *Archives of General Psychiatry* **34**(1), 98–111 (1977)
- [75] Kessler, R.C., McGonagle, K.A., Swartz, M., Blazer, D.G., Nelson, C.B.: Sex and depression in the National Comorbidity Survey I: Lifetime prevalence, chronicity and recurrence. *J Affective Disorders* **29**(2), 85–96 (1993)
- [76] Grigoriadis, S., Robinson, G.E.: Gender issues in depression. *Ann Clin Psychiatry* **19**(4), 247–255 (2007)
- [77] Branco, A.C.C.C., Yoshikawa, F.S.Y., Pietrobon, A.J., Sato, M.N.: Role of histamine in modulating the immune response and inflammation. *Mediators of Inflammation* **2018**, 9524075 (2018)
- [78] Rocha, S.M., Pires, J., Esteves, M., G.Baltazar, Bernardino, L.: Histamine: a new immunomodulatory player in the neuron-glia crosstalk. *Frontiers in Cellular Neuroscience* **8**(120) (2014)
- [79] Rocha, S.M., Saraiva, T., Cristovao, A.C., Ferreira, R., Santos, T., Esteves, M., Saraiva, C., Je, G., Cortes, L., Valero, J., Alves, G., Klibanov, A., Kim, Y.-S., Bernardino, L.: Histamine induces microglia activation and dopaminergic neuronal toxicity via H1 receptor activation. *Journal of Neuroinflammation* **13**(1), 137 (2016)